8-2019

# Simple Photochemical Reduction of Carbon Dioxide to Formate

Ovuokenye Omadoko
*East Tennessee State University*

# Simple Photochemical Reduction of Carbon Dioxide to Formate

---

A thesis

presented to

the faculty of the Department of Chemistry

East Tennessee State University

In partial fulfillment

of the requirements for the degree

Master of Science in Chemistry

---

by

Ovuokenye Omadoko

August 2019

---

Dr. Dane Scott

Dr. Scott Kirkby

Dr. Marina Roginskaya

Dr. Greg Bishop

Keywords: Carbon dioxide, Titanium dioxide, Formate, Metal phthalocyanine

ABSTRACT

Simple Photochemical Reduction of Carbon Dioxide to Formate

by

Ovuokenye Omadoko

There is a need to develop techniques for conversion of carbon dioxide to other useful products such as methanol, formaldehyde, formic acid, formate, methane, and hydrocarbons. Carbon dioxide can be converted into these products using different methods such as photochemical, electrochemical, thermochemical and hydrogenation by bacteria. Formate is of interest due to its wide industrial applications which include it's use in direct liquid fuel cells, as an additive in pyrolysis vapors, a precursor for biological fuels, and it is a key intermediate in methanogenesis breaking down complex organic compounds. In this work, conversion of carbon dioxide to formate was accomplished photochemically. The concentration of formate obtained was quantified using ion chromatography. The yield of formate, based on the amount of carbon dioxide in solution, was 1.54%, while the quantum yield was near 2.0%. Detailed studies of the photoreduction process showed that the amount of sensitizer, light intensity and pH affect the amount of formate generated.

# DEDICATION

This work is dedicated to God Almighty; my parents, Patrick and Joyce Omadoko; my siblings, Ogaga Omadoko, Uzezi Omadoko, Tobore Omadoko, Efemena Omadoko; my uncles, William Onakpoma, Kachi Onuoha; my aunty, Funmi Obaseki and my best friends, Adeniji Elisha, Chimdi Kalu, Samson Olowoyo, Esther Alorkpa and everyone who has supported me during my program.

ACKNOWLEDGEMENTS

I wish to express my sincere gratitude to my research advisor, Dr Dane Scott for his encouragement and support towards the success of my research work. I would also like to thank my great lab partner, Mr. Sami Mohammed Alharbi. I would also like to express my appreciation to my program coordinator, Dr. Marina Roginskaya, for her counsel, and Dr. Scott Kirkby and Dr. Greg Bishop for being part of my advisory committee.

TABLE OF CONTENTS

LIST OF TABLES

Table Page

LIST OF FIGURES

Figure Page

# LIST OF ABBREVIATIONS

| Abbreviation | Description |
|---|---|
| $CO_2$ | Carbon dioxide |
| $TiO_2$ | Titanium dioxide |
| $H_2SO_4$ | Sulfuric acid |
| DFPFC | Direct formate – peroxide fuel cell |
| PC | Phthalocyanine |
| MPC | Metal phthalocyanine |
| InPC | Indium phthalocyanine |
| CuPC | Copper phthalocyanine |
| NiPC | Nickel phthalocyanine |
| ZnPC | Zinc phthalocyanine |
| CoPC | Cobalt phthalocyanine |
| NADPH | Nicotinamide adenine dinucleotide phosphate |
| ATP | Adenosine triphosphate |
| PS | Photosystem |
| EWG | Electron-withdrawing group |
| EDG | Electron-donating group |

| | |
|---|---|
| HOMO | Higher occupied molecular orbital |
| LUMO | Lower unoccupied molecular orbital |
| PDT | Photodynamic therapy |
| DSSC | Dye-sensitized solar cell |
| $S_0$ | Ground state |
| $S_1$ | First singlet excited state |
| $S_2$ | Second singlet excited state |
| IC | Ion chromatography |
| CB | Conduction band |
| VB | Valence band |
| N | Number of electrons |
| n | Number of moles of product |
| F | Faraday's constant |
| Q | Charge in coulombs |
| f | Faradaic efficiency |
| $\phi$ | Quantum yield |
| q | Moles of photons emitted per unit time |
| t | Irradiation time |
| l | Optical pathlength |

| | |
|---|---|
| h | Hour |
| min | Minute |

# CHAPTER 1

# INTRODUCTION

## Carbon Dioxide

The rich energy nature, availability, and stability of common fossil fuels including natural gas, petroleum, and coal have made fossil fuels primary energy sources.[1,2] Industrialized countries such as the USA and China have relied greatly on the use of coal as a major energy source over the years.[1,3,4] Continuous dependence on fossil fuel burning has globally increased the atmospheric concentration of $CO_2$, a major anthropogenic greenhouse gas, to 409.14 ppm in 2019.[5] Industrialized countries are working towards reducing fossil fuel consumption for power production.[6–8] Examples are use of biomass, geothermal, steam, solar, hydroelectric, nuclear and wind power.[6–8]

Carbon dioxide is a stable component of the ambient air and a contributor to global warming.[9–11] Global warming is due to the greenhouse effect which occurs because of the absorption and re-emission of infrared radiation by $CO_2$.[10] Reduction of the amount of atmospheric $CO_2$ will minimize the danger of global warming and conversion to renewable fuels could improve sustainable technologies.[11,12] Hence, there is an interest in removing or reducing $CO_2$ to other products.[13,14] There are different strategies for lowering $CO_2$ levels such as carbon capture and conversion to other products such as formate.[15]

## Carbon Dioxide Capture

Carbon dioxide capture is ideal at sites where fossil fuels are used.[16,17] Atmospheric $CO_2$ can be captured through either absorption or adsorption processes. Alkanolamine compounds are widely used for absorption of $CO_2$.[16,18] Alkanolamine reacts with the $CO_2$ to form soluble carbamate and

bicarbonate. Heating the mixture formed above 100 °C regenerates the alkanolamine and $CO_2$ is reclaimed. The reaction of alkanolamine with $CO_2$ is given in Equations 1.1-1.2.[16]

$$2RR^1NH + CO_2 \longleftrightarrow RR^1NCOO^- + RR^1NH_2^+ \quad (1.1)$$

$$RR^1NCOO^- + H_2O \longleftrightarrow RR^1NH + HCO_3^- \quad (1.2)$$

The $CO_2$ absorption capture process is a chemical absorption process, which requires high amounts of energy to recover $CO_2$. Other disadvantages in using $CO_2$ absorption capture include corrosion and needing a large volume of absorber.[17] Adsorption of $CO_2$ is an alternative.

Adsorption makes use of adsorbents to capture atmospheric $CO_2$.[17,19] Such adsorbents bind with $CO_2$ physically (physisorption) or chemically (chemisorption).[16,19] Carbonaceous materials (graphene, carbon nanotube, activated charcoal), zeolite, ordered mesoporous silica, metal-organic frameworks have been reported as good physical adsorbents while amine-based materials (amine-grafted by toluene reflux), lithium-based materials and calcium-based materials are good chemical adsorbents.[17] Both physical and chemical adsorption require less energy for regeneration of $CO_2$ as compared to chemical absorption.[17] The adsorption of $CO_2$ on the surface of the adsorbent has been experimentally determined to be influenced by various factors such as surface area, partial pressure of $CO_2$ and surface pH.[20]

## Properties of Carbon Dioxide

The solubility of a gas in a solvent is a measure of the volume of gas dissolved in one gram of solvent. Solubility depends on certain factors such as temperature, pressure and the nature of the solvent.[21] Carbon dioxide dissolves more in alkaline medium than acidic medium because carbon dioxide reacts easily with alkaline solution to form bicarbonate.[17]

According to an experimental report on solubility of $CO_2$ in sulfuric acid, about 0.7 $cm^3$ of $CO_2$ is required to saturate one gram of 1.0 mM $H_2SO_4$.[22] The solubility can be used to determine the theoretical yield of formate from photoreduction of $CO_2$.[23] The development of innovative processes for $CO_2$ recycling appears to be gaining more interest due to reduction of $CO_2$ into useful industrial products such as methane, ethylene, alcohols, formaldehyde, formic acid and formate.[24] These processes are based on photochemical, electrochemical, thermochemical, and biological hydrogenation.[25,26]

## Thermochemical Reduction of Carbon Dioxide

One effective though expensive method of $CO_2$ reduction to other valuable products is thermochemical reduction. This method involves the use of heat treatment at moderate temperatures in the presence of alkali metal hydrides such as lithium hydride (LiH) or sodium hydride (NaH).[27] This method produces methane and hydrogen gas.[27] The amount of methane and hydrogen gas produced depends on the temperature and time of the reaction.[27] It has also been reported that amorphous carbon plays an important intermediate role in the process of thermochemically converting $CO_2$ to methane and hydrogen gas.[27]

## Biocatalytic Reduction of Carbon Dioxide

Another effective method of converting $CO_2$ into formate and other products is biocatalysis, which involves the hydrogenation of $CO_2$ by a bacterial $CO_2$ reductase under the influence of high temperature and pressure.[28–30] Use of $CO_2$ reductase enzymes is highly selective under mild conditions.[28]

However, most biocatalysts require other coenzymes such as nicotinamide adenine dinucleotide phosphate (NADPH) or hydrogen gas to effectively hydrogenate $CO_2$ to formate.[29]

Examples of bacteria that produce such enzymes include *Methylobacteria jeotgali, Methylobacteria platani*, and *Methylobacteria dankookense*.[31] These biocatalysts come from anaerobic organisms that are not very stable when in contact with oxygen, and this can be a major obstacle for biocatalytic reduction of $CO_2$ because of enzyme reusability problems under such conditions.[32,33] Acetogenic bacteria have been observed to be the only microorganism that can receive electrons from electrode surfaces to effectively enhance reduction of $CO_2$ while others require coenzymes such as NADPH to enhance the movement of electrons between enzymes and electrodes.[34]

There are several reports of the use of nanostructures at electrode interfaces to reduce the distance between enzymes and the electrode to increase the chance of effective transfer of electrons.[34] Limitations have been observed in biocatalytic reduction, though the reaction has applications in the development of biosensors and bioreactors.

## Electrochemical Reduction of Carbon Dioxide

Electrochemical reduction of $CO_2$ depends on several factors such as the nature of the cathode, the electrolyte used, pressure, and temperature of the system.[35] For instance, it has been reported that mixtures of hydrocarbons (mainly methane and ethylene) and alcohols are obtained when a metal like copper is used as the cathode, the use of zinc, silver, or gold will yield mainly carbon monoxide while other moderately reactive metals like tin, mercury, or lead are strictly used for production of formic acid and formate through electrolysis.[35] The faradaic efficiency, f, of an electrochemical cell is calculated by Equation 1.3.[36]

$$\mathrm{f} = \frac{nNF}{Q} \tag{1.3}$$

where '$n$' represents moles of product formed during the electrochemical process, '$N$' represents number of electrons required for the formation of one mole of product from $CO_2$, (N = 2 for formate

formation), '*F*' is Faraday's constant (96,500 C $mol^{-1}$ of electrons) and '*Q*' is total charge in coulombs of electricity required for the electrochemical process.[37]

Electrocatalysts for electrochemical reduction of $CO_2$ have problems such as low efficiency due to hydrogen evolution, requiring a high over potential, are easily deactivated, and have poor selectivity for products.[38] For instance, electrochemical reduction of $CO_2$ to formate using tin has been reported to have a faradaic efficiency of 58%, while another report shows a faradaic efficiency of 18% using tin particles on carbon paper.[38,39] During electrochemical reduction of $CO_2$, the electrolyte used is usually saturated with $CO_2$ before the process begins.[38,39] Also, $CO_2$ is continuously bubbled at a constant flow rate while applying a constant overpotential.[38,39] Additionally, $CO_2$ is reduced naturally through photosynthesis.[40]

## Carbon Dioxide and Photosynthesis

Photosynthesis occurs in sub-cellular structures in plants called chloroplasts.[41] The chloroplast contains chlorophyll, a green pigment which carries out the photosynthesis process.[41] The major functions of chlorophyll in photosynthesis include absorbing light, transferring excitation energy to reaction centers, charge separation across the photosynthetic membrane and producing membrane potential leading to adenosine trisphosphate (ATP) and NADPH.[42–44]

Photosynthesis is a natural photoreduction process involving a series of biochemical reactions in which green plants and algae convert light and $CO_2$ into glucose and oxygen, releasing energy in the form of ATP in the presence of sunlight trapped by a chromophore called chlorophyll.[40] Photosynthesis is generally represented by the Equation 1.4.[40]

$$6CO_2 + 6H_2O \rightarrow C_6H_{12}O_6 + 6O_2 \quad (1.4)$$

Antenna chromophores have been reportedly applied to extend photosynthesis to regions where chlorophyll is not present.[40] Examples of such antenna chromophores include carotenoid polyenes, phycoerythrin, phycocyanin, porphyrins, and cyclic tetrapyrroles.[45–47]

Photosynthesis occurs under illumination (light-dependent reaction) and dark conditions (light-independent reaction).[42,48] The light dependent reaction occurs in three phases; light absorption, primary electron transfer, and formation of NADPH and ATP.[41,48,49] The dark reaction involves synthesis and exportation of stable products in which the formed ATP and NADPH are used to reduce $CO_2$ into simple sugar.[41,46,47]

In the light reaction stage, photons are absorbed by antenna chlorophyll systems; photosystem I (PS I) and photosystem II (PS II), leading to excitation of a chlorophyll pair and resulting in the splitting of water as shown in Equation 1.5.[50,51]

$$H_2O \longrightarrow \frac{1}{2}O_2 + 2H^+ + 2e^- \quad (1.5)$$

The high energy excited electrons pass through an electron transport chain and pump protons in the lumen and reduce $NADP^+$ to NADPH in PS I as shown below.[50]

$$NADP^+ + H^+ + 2e^- \longrightarrow NADPH \quad (1.6)$$

The protons generated from water and those pumped into the thylakoid membrane, drive the production ATP from ADP.[50]

$$ADP + H_3PO_4 \longrightarrow ATP + H_2O \quad (1.7)$$

During the light independent reaction, ATP and NADPH are consumed to reduce $CO_2$ to glucose.[50–52]

$$6CO_2 + 12NADPH + 12H^+ + 18ATP + 12H_2O \longrightarrow C_6H_{12}O_6 + 12NADP^+ + 18ADP + 18H_3PO_4 \quad (1.8)$$

A reaction scheme of natural photosynthesis is shown in Figure 1.[53]

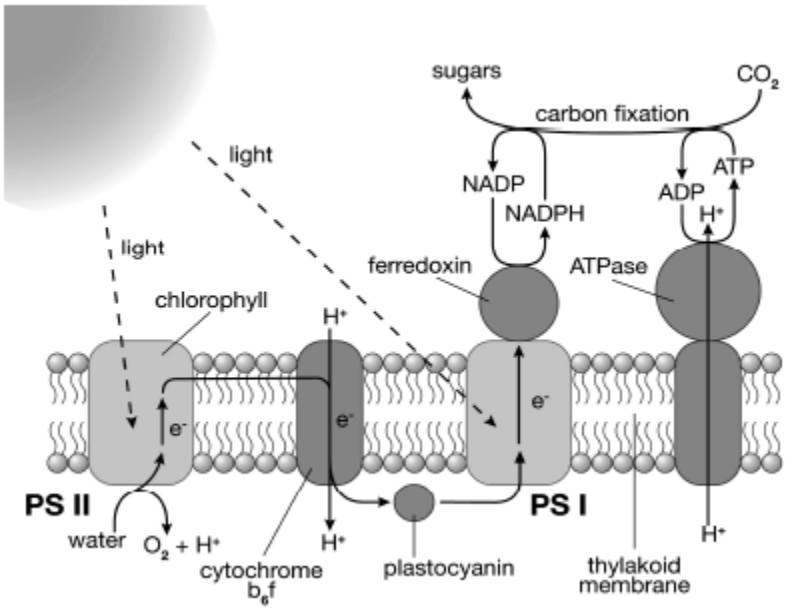


Figure 1. Scheme for natural photosynthesis process[53]

(Reprinted with permission from Muckerman, J.; Fujita, E. Artificial Photosynthesis. In ACS Symposium Series; American Chemical Society, 2009; Vol. 1025, pp 283–312.)

In photosynthesis, about 75% of the incident solar energy is lost in absorbing light due to reflection, transmission, or conversion to heat.[54] The quantum yield of products formed per photon absorbed during natural photosynthesis is approximately 1%.[41,51]

## Chlorophyll

The natural pigments in plants that act like phthalocyanines are chlorophylls.[54] Chlorophyll is made up of tetrapyrrole ring with magnesium as the center atom.[54] There are four different types of chlorophyll; chlorophyll a, b, d and f.[55] Figure 2 below shows the chemical structures of chlorophyll a and chlorophyll f and their absorption spectra.[56]

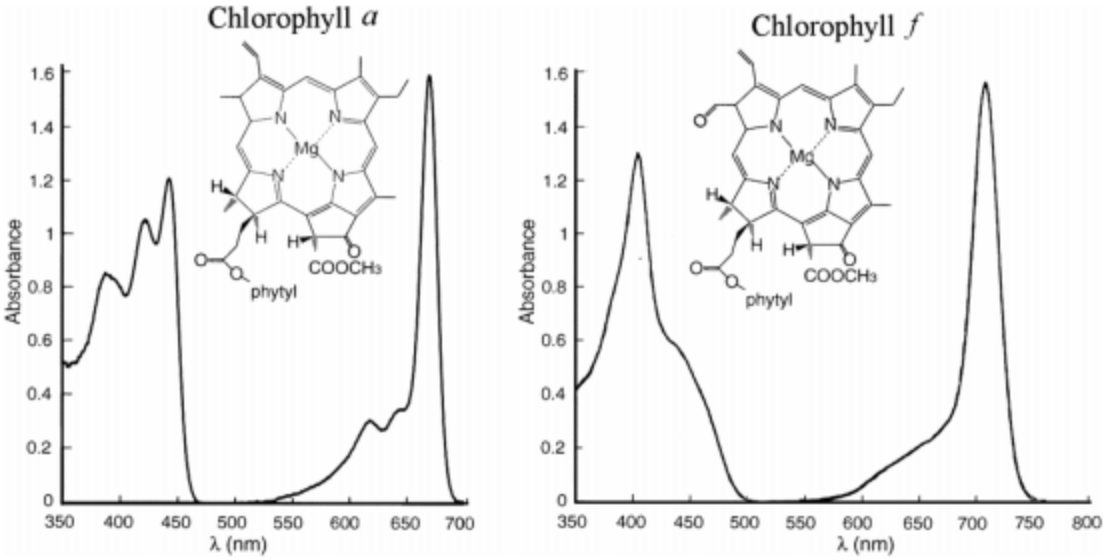


Figure 2. Chemical structures and absorption spectra of chlorophyll a and chlorophyll f[56]

(Reprinted with permission from Li, Y.; Cai, Z.-L.; Chen, M. Spectroscopic Properties of Chlorophyll F. *J. Phys. Chem. B* **2013**, 117 (38), 11309–11317.)

From the spectra, it can be seen that chlorophyll generally has two prominent absorption bands, a B band in the near UV or blue region and a Q band in the near-infrared or red region.[41,56,57] The difference in absorption spectrum of chlorophyll a and chlorophyll f is due to the minor chemical structural modification.[56] This causes a difference in molecular electronic energies.[56] The presence of antenna chromophores like carotenoid complexes (accessory pigments) in green plants aid the absorption of light within the spectral region where chlorophyll can't absorb.[54] However the antenna complexes can't perform charge separation but transfer the energy to a chlorophyll sensitizer.[54] An efficient antenna must allow electron transfer for $CO_2$ reduction to occur.[45] Chlorophyll functioning as a sensitizer in natural photosynthesis process, makes the photoreduction of $CO_2$ to simple sugar possible.[54]

An artificial photochemical process is capable of reducing $CO_2$.[58–61] This method has gained interest due to adequate availability of sunlight to convert $CO_2$ into various chemical products in a more carbon-friendly way.[58] Reduction of $CO_2$ occurs by using a semiconductor photocatalyst enhanced by a sensitizer which absorbs photons.[58–61] Several photocatalysts such as titanium dioxide ($TiO_2$), zinc oxide (ZnO), zirconium dioxide ($ZrO_2$), and gallium oxide ($Ga_2O_3$) have been reported to be used in the photoreduction of $CO_2$ into several products.[58] The choice of $TiO_2$ as a catalyst for $CO_2$ photochemical reduction is common due to its low toxicity, low cost, availability, moderate activity, and high ability to resist photocorrosion.[59,61]

## Titanium Dioxide

The most useful titanium product from titanium ore is titanium dioxide ($TiO_2$).[62] Crystalline $TiO_2$ exists in three major forms in nature: rutile, anatase, and brookite.[63] Rutile was discovered by Werner in 1803, brookite was discovered in 1825 by Levy, and anatase was discovered in 1801 by Havy.[64]

These forms of $TiO_2$ phases are made up of $TiO_2$ octahedra where each oxygen atom is surrounded by three titanium atoms and six oxygen atoms around each titanium atom.[63,65] The crystalline structure of the three phases are different due to octahedral distortions caused by the oxygen atoms around each titanium atom.[65] Rutile has the least distortion and brookite has the greatest distortion, making it least stable, difficult to manufacture and not common.[63] Rutile and anatase are tetragonal while brookite is orthorhombic.[64] Rutile is the most available form of $TiO_2$.[62] Figure 3 shows the three crystalline phases of $TiO_2$.[64]

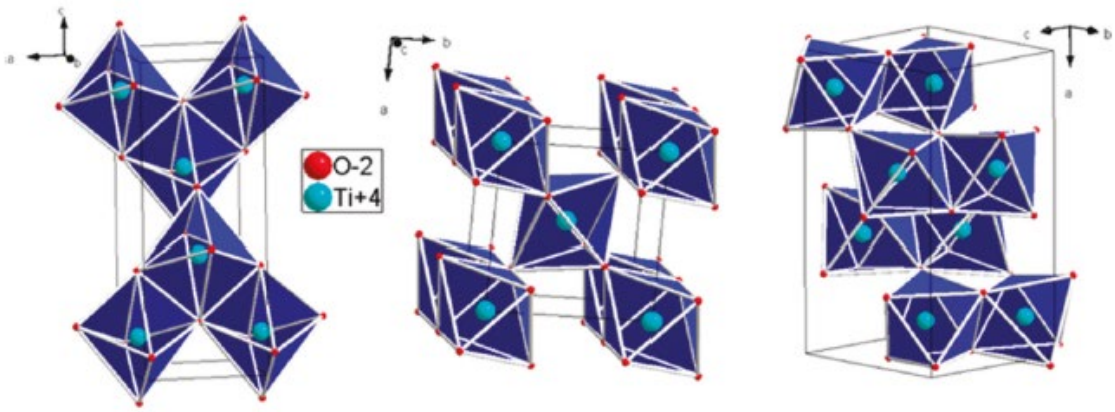


Anatase Rutile Brookite

Figure 3. Representations of the different phases of $TiO_2$: anatase, rutile and brookite[64]

(Reprinted with permission. Dambournet, D.; Belharouak, I.; Amine, K. Tailored Preparation Methods of $TiO_2$ Anatase, Rutile, Brookite: Mechanism of Formation and Electrochemical Properties. *Chem. Mater*. **2009**, 22 (3), 1173–1179.)

The density of the three $TiO_2$ phases varies.[66] Anatase has the lowest density, 3.83 $gcm^{-3}$, compared to brookite, 4.17 $gcm^{-3}$, and rutile, 4.24 $gcm^{-3}$.[51] Also, the refractive index of anatase is 2.5688 and rutile is 2. 9467.[66] Refractive index determines how scattering of light varies between each phase. Refractive index depends on particle size. Rutile particle size is 0.25 microns resulting in the highest amount of scattering of visible light when compared to anatase particle sizes of about 0.3 microns.[62]

Pure $TiO_2$ crystals are white but sometimes appear red, yellow, black or brown due to the presence of impurities like iron, chromium, vanadium, or niobium.[65] Rutile can be reddish brown, yellowish, bluish, or violet.[64] Brookite ranges from dark brown to greenish black while anatase varies from black to reddish brown or yellowish brown.[64,67] Anatase has a lower melting point and transforms into the rutile phase at temperatures above 600 °C.[68] During the transformation of anatase

to rutile at higher temperatures, pseudoclose – packed planes of oxygen and close – packed planes of rutile are retained.[69]

The relative phase stability changes with particle size due to surface energy effects.[70] Anatase is the most stable when particle size is less than 11 nm. Between 11 nm and 35 nm, brookite will be the most stable while rutile becomes more stable when the particle size exceeds 35 nm.[71] Though rutile tends to be the most thermodynamically stable, anatase has been reported to be more active due to having higher surface area, charge mobility and exciton diffusion length.[64,72]

$TiO_2$ has been synthesized from titanium ore through several methods such as hydrolysis, flame pyrolysis, sol-gel, chemical vapor deposition, physical vapor deposition and micro-emulsion.[62,71] The hydrolysis method is preferable because synthesis is at ambient pressure and temperature.[62] Hydrolysis can be carried out using a sulfate or chlorine process.[64,73]

## Photoactivity and Modification of Titanium Dioxide

Titanium dioxide's electronic structure has an empty conduction band and filled valence band.[71] The energy difference between the valence band and conduction band is called the band gap.[71] Irradiation of $TiO_2$ with light energy equal to or greater than the band gap causes electron excitation from the valence band to the conduction band and leaving charged holes in the valence band.[71] A redox process is induced by reaction of photogenerated electrons and holes with electron donors and acceptors adsorbed on $TiO_2$ surface.[66] The difference in electronic structure of the various $TiO_2$ phases affects the band gap and electron transfer ability. Anatase has an indirect band gap of 3.2 eV while rutile has a direct band gap of 3.0 eV.[66,74]

$TiO_2$ can only absorb UV radiation due to the large band gap between the conduction and valence bands.[60] To extend absorption to the visible region, $TiO_2$ is modified by doping with materials such as non-metals,[75–78] metals,[11] or dyes.[11,79,80]

## Non-Metal Modification of $TiO_2$

P-block non-metals such as carbon,[81] flourine,[82] nitrogen,[83] and sulfur[84] have been reportedly used in modification of $TiO_2$ to enhance the photocatalytic properties of $TiO_2$. Modification with a non-metal has been reportedly found to be more efficient in increasing photocatalytic efficiency of $TiO_2$ when compared to metal doping.[83,85] This is due to the fact that a non-metal does not form recombination centers.[66] The photoactivity of the modified $TiO_2$ can be influenced by the ionic radius of the non-metal.[83] According to reported experiments, nitrogen-modified $TiO_2$ shows increased photoactivity compared to using non- metals like fluorine, nitrogen, phosphorus, sulfur and carbon due to the influence of the p-states on narrowing the band gap of $TiO_2$.[83]

## Metal Modified $TiO_2$

Metal modification involves adsorption to the crystal lattice of the $TiO_2$ semiconductor. When a metal is adsorbed into $TiO_2$, electrons flow to the metal until the Fermi energy levels of the metal and $TiO_2$ reach equilibrium.[66,69] The causes an upward bend of the valence band of $TiO_2$ which creates a Schottky barrier.[66,86] This barrier trap acts as an electron scavenger preventing crossing of electrons back to $TiO_2$ resulting in recombination.[69] Figure 4 below shows metal modified $TiO_2$ and electron-hole generation due to absorption of UV radiation.[69]

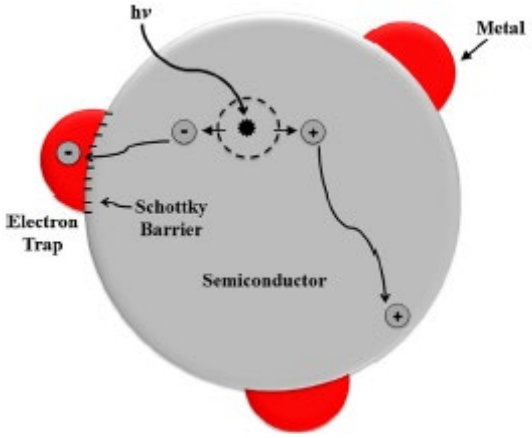


Figure 4. Metal modified $TiO_2$ semiconductor.[69]

(Reprinted with permission from Ola, O.; Maroto-Valer, M. M. Review of Material Design and Reactor Engineering on $TiO_2$ Photocatalysis for $CO_2$ Reduction. *J. Photochem. Photobiol. C Photochem. Rev.* **2015**, 24, 16–42.)

Photogenerated electrons diffuse to adsorbed surface species for photoreduction. According to a report on $CO_2$ reduction to methanol, increasing the ratios of Ag/ $TiO_2$ under 254 nm UV radiation over a period of 24 h results in more methanol.[87] This is due to the fact that Ag causes the Fermi level of $TiO_2$ to be higher enhancing electron transfer from the conduction band of $TiO_2$ to silver. Also, Schottky barrier formation enhances electron trapping improving quantum efficiency.[87]

## Dye-Sensitized Titanium Dioxide

Dye sensitization of $TiO_2$ increases the absorption of $TiO_2$ towards visible light.[64,66,88,89] Various dyes reportedly used as sensitizers include porphyrins, rhodamine B, Rose Bengal, thionine, and phthalocyanines (PCs).[66,90,91] Such dyes have high absorption in the visible region, and the excited state has a long life time.[61,66,92] Photogenerated electrons are transferred from an excited state of the dye molecule to the conduction band of $TiO_2$ as shown in Figure 5.[69]

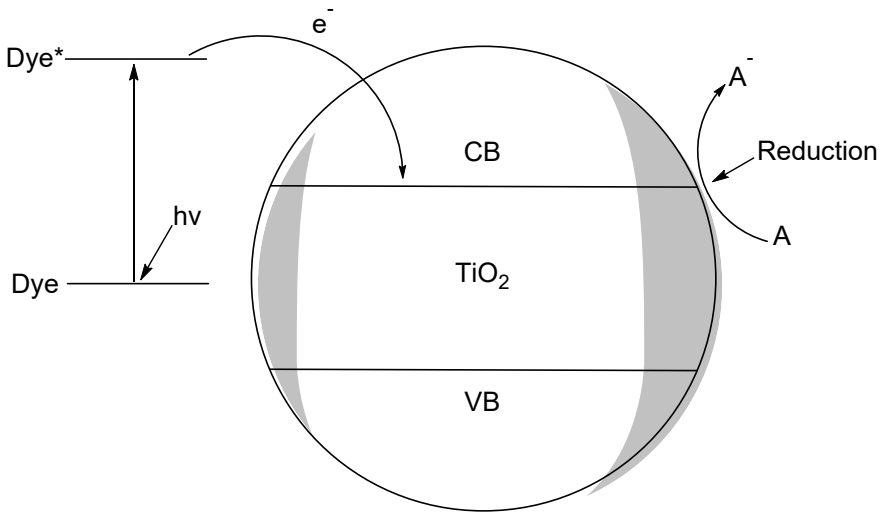


Figure 5. Dye sensitized $TiO_2$ where A is the electron acceptor[69]

The transferred electrons reduce $CO_2$ adsorbed on the $TiO_2$ surface.[67] The photosensitizer must be able to undergo fast electron injection into $TiO_2$ to maximize photoefficiency and prevent recombination.[66,69,88] The rate of electron migration to $TiO_2$ is influenced by the properties of $TiO_2$ and surface interaction with the dye.[67] Titanium dioxide has a high surface area, suitable conduction band just lower than the dye, high stability with high refractive index, which has been reported to facilitate injection of electrons from the excited state of dyes to the conduction band of $TiO_2$.[66,69,93]

PCs have been used as sensitizers to promote the activation of $TiO_2$ as a photocatalyst due to their high stability, low cost, low environmental impact, and high efficiency in energy conversion.[94–98]

## Metal Phthalocyanines

The first reported synthesis of PC was in 1907 when Braun and Tcherniac accidently isolated a blue complex compound as a by-product in attempt to synthesize ortho-cyanobenzamide.[99,100] Twenty years later, H. de Diesbach and E. von der Weid synthesized the first copper phthalocyanine by reacting a mixture of o-dibromobenzene, pyridine and cuprous cyanide.[101] X-ray diffraction was

used by Robertson to determine the crystalline structure of prepared Cu, Ni, and Pt phthalocyanines in 1935.[102]

The PC molecule contains four indoline units linked by nitrogen atoms in a planar structure with a conjugated system of eighteen π-electrons.[97] PC can be classified as synthetic analogues of natural porphyrin products such as chlorophyll and hemoglobin due to their similar structure.[94,103] PCs are also called tetrabenzoporphyrazins.[94] Metal PCs are denoted as $MC_{32}H_{16}N_8$ or MPCs.[97] Figure 6 shows the structure of PC without and with a metal center.[103]

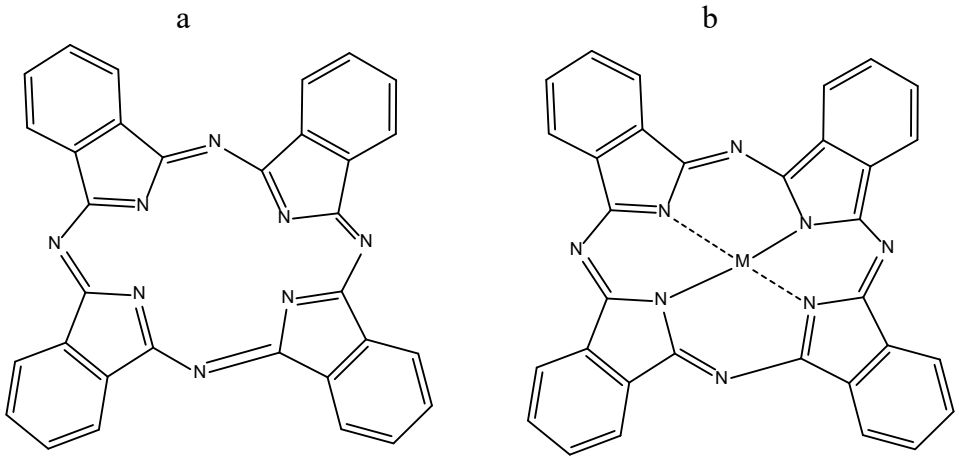


Figure 6. Structure of (a) phthalocyanine and (b) metal phthalocyanine[103]

Several synthetic procedures have been reported for MPC and $H_2PC$. One reported method for MPC synthesis involves a condensation reaction of urea with phthalic anhydride in the presence of a metallic chloride. Metal-free phthalocyanine was prepared by heating a metal amylate with phthalonitrile followed by removing the metal center by heating in methanol.[103]

## UV-Visible Absorbance of Phthalocyanines

Phthalocyanines have a more delocalized system when compared to porphyrins leading to a higher probability of π-π* transitions when illuminated with UV-Vis light.[98] MPCs have specific Q and B absorption bands within the UV-Vis region.[104,105] The Q-band absorption can be found within wavelengths of 600-800 nm in the visible region while the B-band is from 300-500 nm in the UV region.[105] The Q-band absorption is assigned to the ground state π-π* electronic transition from the highest occupied molecular orbital (HOMO) to the lowest unoccupied molecular orbital (LUMO) of the MPCs ($S_o \rightarrow S_1$).[104–107] The B-band is due to a strong π-π* energy level transition from HOMO to higher excited state ($S_o \rightarrow S_2$).[106–109] All MPCs have been shown to have a prominent narrow Q-band and a relatively weaker B-band.[104–106,108] Figure 7 shows the UV-Vis absorption spectra of ZnPC in ethanol ($1 \times 10^{-5}$M) with molar absorptivity of $1 \times 10^{-5}$ $cm^{-1}$ $M^{-1}$ and maximum absorption at 673 nm.[106]

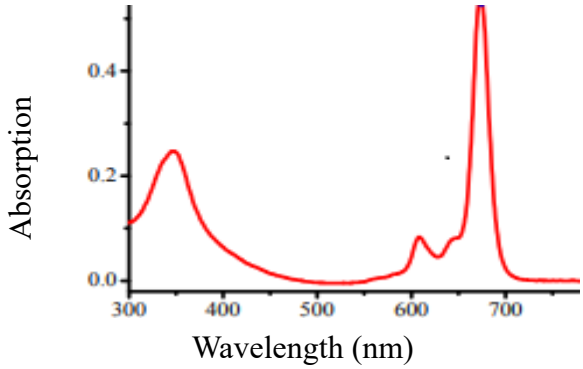


Figure 7. UV-Vis absorption spectra of ZnPC in ethanol[106]

(Reprinted with permission from Tiwari, A.; Krishna, N. V.; Giribabu, L.; Pal, U. Hierarchical Porous $TiO_2$ Embedded Unsymmetrical Zinc–Phthalocyanine Sensitizer for Visible-Light-Induced Photocatalytic $H_2$ Production. *J. Phys. Chem. C* **2017**, 122 (1), 495–502.)

The variation in different MPCs wavelength of maximum absorption is due to the difference in the energy gap between the HOMO and LUMO of the MPCs delocalized system.[108] An increase in valence electrons of the center metal leads to a higher electron density of the MPCs conjugated system and lower gap.[108,110] This causes a bathochromic shift. The presence of electron-withdrawing (EWG) or electron-donating groups (EDG) substituted onto the MPC ring influences the Q-band.[110] An EDG increases electron density of the delocalized system lowering the band gap and shifts absorption to longer wavelengths (red or bathochromic shift). An EWG causes absorption to shift toward shorter wavelengths (blue or hypsochromic shift).[111] The photochemical reduction of $CO_2$ to formate in the presence of $TiO_2$ activated by various metal phthalocyanines (ZnPC, NiPC, InPC, and NiPC) in solution is the subject of this research.

## Properties of Phthalocyanines

Physical properties of phthalocyanines depend on having a metal center and if there are substituents.[96,97] Phthalocyanines range in color from dark blue to green.[97] Metallophthalocyanines have a high melting point.[112] For example, NiPC melts at 300 ℃.[113] Phthalocyanines are quite insoluble in water due to their π-π* conjugation system.[114] They tend to be soluble in sulfuric, phosphoric, hydrofluoric, trichloroacetic acids and most organic solvents such as dichloromethane, dimethyl formide and dimethyl sulfoxide.[94,115] Solubility of MPCs can be improved by linking ligands with hydrophilic groups such as sulfonates,[116] phosphate,[117] amino,[118] carboxylate,[119] or carbonyl groups.[86] Solubility of PCs decrease due to aggregation caused by interactions between their 18 π delocalized electrons.[120] The degree of aggregation depends on the central metal ion, type of substituents on the ligands, temperature, and the nature of the solvent.[120,121] Methods reportedly used to reduce aggregation of PCs include using water soluble groups, dendrimer and surfactant

substituents as axial ligands.[115,119] Such bulky substituents prevent delocalized π-electrons from interacting and reduces aggregation.[122]

## Phthalocyanines as Photosensitizers

PC molecules become excited when they absorb light. Excited PCs molecules can react when oxidizing agents are present and decompose.[96] Photochemical decomposition of PCs in solution is regarded as a complex process due to several radicals that could be formed.[96] When exposed to UV-Vis radiation, weakening of carbon-nitrogen bonds may occur resulting in photodegradation of MPCs.[96] One possible degradation product is phthalimide.[96] The presence of a solvent influences the photostability of PCs due to interaction with PC ligands. Experiments show that electron rich ligand substituents such as hydroxyl groups, ethylene glycol, and amine increase the electron density of the carbon-nitrogen bond which enhances stability.[123] The photostability of PCs also depends on the molecular structure and nature of the bond between the metal and ligands. The electronic configuration and electronegativity of PCs complexed with metal influences the carbon-nitrogen bond lengths resulting in different stabilities when illuminated with UV-Vis radiation.[96] Experiments show solid PCs bind $O_2$ or $N_2$ causing a change in electron density distribution and polarizability within the PC, which results in a decrease in carbon-nitrogen bond length.[96]

## Applications of Phthalocyanines

The color, high thermal stability and conductivity of MPC's has made them suitable for many applications in dyes, medicine, ecology and chemical catalysis.[96,124] MPCs account for about 90-95% of blue and green chemicals used in production of inks, paints, dyes, and plastics.[96]

In medicine, MPCs have been applied in photodynamic therapy (PDT), a special kind of phototherapy technology used in treatment of skin diseases and malignant tumors.[124–126] The

operation of PDT is based on the use of photosensitizers like soluble MPCs, light and $O_2$ to cause a photoinduced chemical reaction generating singlet oxygen that destroys harmful cells while minimizing the effects on normal cells.[124–126]

MPCs have also been reportedly applied in ecology for pollution degradation.[127,128] An example of this is $TiO_2$ nanoparticles sensitized with cobalt phthalocyanine (CoPC) for photodegradation of 4-chlorophenol. Electrons transferred from CoPC in an excited state to $TiO_2$ react with $O_2$ to produce singlet $O_2$.[127,128] Singlet $O_2$ then reacts with hydrogen peroxide to form hydroxyl radicals.[127,128] The hydroxyl radicals formed react with 4-chlorophenol to form chlorocatechol and chlorobenzoquinone.[127,128] Subsequent attack of hydroxyl groups on chlorobenzoqunone results in conversion to simple acids.[127,128]

Another use of MPCs is in dye-sensitized solar cells (DSSCs).[129–131] DSSCs are made up of a photosensitizer and semiconductor nanoparticles as the working electrode, a redox mediator and counter electrode.[129,130] DSSCs absorb solar photons, generate charge carriers and transfer charge from the sensitizer excited state into the conduction band of the semiconductor.[129] This enhances solar energy conversion to electricity.[129,130] The redox mediator reduces the oxidized sensitizer. An example of this is a ZnPC photovoltaic cell with carboxylic acid groups resulting in 4.1% photovoltaic efficiency.[129,131] The presence of carboxylic acid as anchoring groups prevents the dissociation of ZnPC from $TiO_2$ causing a decrease in conversion of photons to electrons.[129,131]

## Photochemical Reduction of Carbon Dioxide Using Dye Sensitized $TiO_2$

Carbon dioxide can also be reduced photocatalytically by photosensitized $TiO_2$ systems.[132] Photoreduction of $CO_2$ to formate involves absorption of photons by a sensitizer, such as MPC, in the electronic ground state which is highly reactive.[132] Absorption of light energy equal or greater

than the band gap of the sensitizer initiates excitation of electrons from the valence band to the conduction band.[132] Excited electrons are injected into the conduction band of $TiO_2$, and electron transfer reactions occur on the surface where $CO_2$ is adsorbed.[132] A possible product is formate. The photoreduction process of carbon dioxide to formate under acidic medium can be represented by Equations 1.9-1.15.[133–136]

$$MPC + h\nu \rightarrow MPC^* \quad (1.9)$$

$$MPC^* + TiO_2 \rightarrow e^- \cdot TiO_2 + MPC^+ \quad (1.10)$$

$$CO_2(g) + e^- \cdot TiO_2 \rightarrow TiO_2 \cdot CO_2^-(ads) \quad (1.11)$$

$$e^- \cdot TiO_2 + H^+(aq) \rightarrow TiO_2 \cdot H(ads) \quad (1.12)$$

$$TiO_2 \cdot CO_2^-(ads) + TiO_2 \cdot H\,(ads) \rightarrow TiO_2 \cdot HCO_2^-(ads) \quad (1.13)$$

$$TiO_2 \cdot HCOO^-(ads) + H^+(aq) \rightarrow TiO_2 + HCOOH(aq) \quad (1.14)$$

$$2\,MPC^+ + H_2O \rightarrow 2\,MPC + 2H^+(aq) + \tfrac{1}{2}\,O_2(g) \quad (1.15)$$

Equations 1.16-1.24 suggest a mechanism for photoreduction to formate when pH is equal to or greater than 7, and the $TiO_2$ surface is known to be negatively charged.[95,137,138]

$$TiO^- + H_2O \rightarrow TiOH + OH^- \quad (1.16)$$

$$TiO_2 + TiOH \rightarrow TiO_2 \cdot H^+(ads) + TiO^- \quad (1.17)$$

$$MPC^* + TiO_2 \cdot H^+(ads) \rightarrow MPC^+ + TiO_2H(ads) \quad (1.18)$$

$$CO_2(g) + e^- \cdot TiO_2 \rightarrow TiO_2 \cdot CO_2^-(ads) \quad (1.19)$$

$$TiO_2H(ads) + TiO_2 \cdot CO_2^-(ads) \rightarrow TiO_2 + TiO_2 \cdot HCO_2^-(ads) \quad (1.20)$$

$$TiO_2 \cdot HCO_2^-(ads) \rightarrow TiO_2 + HCO_2^-(aq) \quad (1.21)$$

$$MPC^+ + OH^-(aq) \rightarrow MPC + OH^\cdot \quad (1.22)$$

$$TiO_2H(ads) + OH^\cdot \rightarrow TiO_2 \cdot H_2O(ads) \quad (1.23)$$

$$TiO_2 \cdot H_2O(ads) \rightarrow TiO_2 + H_2O(l) \quad (1.24)$$

The sensitized titanium dioxide surface enables the photoreduction of carbon dioxide to formic acid under mild acidic conditions and formate under alkaline or neutral medium. Formic acid is quantified as formate by ion chromatography (IC) technique.

Quantum Yield

Photochemical efficiency describes the percent of absorbed photons that reduce $CO_2$ to products. The adsorption of $CO_2$ on a photocatalyst, influences the photochemical efficiency of $CO_2$ photoreduction. Photochemical efficiency is commonly referred to as the quantum yield (Φ) of reaction. Since two electrons are involved the photoreduction of $CO_2$ to formate, the photochemical efficiency of the reaction is given by Equation 1.23.[139]

$$\Phi_{\text{formate}} = \frac{2(\text{molecules of formate})}{\text{number of photons}} \text{ x } 100\% \quad (1.23)$$

Photochemical efficiency depends on intensity and wavelength of radiation.[139] According to an experiment conducted on $CO_2$ reduction, using UV light (300 nm) a maximum quantum yield of 28% was obtained.[139] In this experiment, 17 μmol of formic acid was formed after two hours.[139] As wavelength was increased to 350 nm, the photochemical efficiency was near zero percent.[139] The quantum yield of products formed per photon absorbed during natural photosynthesis is approximately 1%,[41,51] while a typical artificial photoreduction of $CO_2$ is at or less than 1%.[140] An example of this is an experiment using a Ru(II)-Re(I) bridged supramolecular complex in an aqueous

solution which resulted in a quantum yield of 0.2% over 24 h of irradiation using 546 nm monochromatic light.[140]

One factor that must be considered in determining the quantum yield of heterogenous catalytic systems is scattering and reflection of incident photons.[141] If light is scattered, the absorbance of a sample measured by an instrument is higher than it should be. This has led to use of an apparent quantum yield where all incident photons are used in the calculation instead of the number of photons absorbed by the photocatalyst.[142] Measuring transmittance using an integrating hard sphere allows collecting scatted light caused by a turbid or heterogeneous sample.[143,144] The instrument subtracts the signal due to scattered light resulting in a true absorbance.

In this work, measurement of polychromatic incident photons in the visible range was performed using a calibrated photodiode detector. Photodiodes work based on the photoelectric effect.[145] Photons strike the semiconductor leading to electron excitation from the valence band to conduction band producing electron-hole charge carrier pairs.[145] Electrons and holes remain separated by a strong local electric field.[145] If photon absorption occurs within the depletion region of the photodiode p-n junction, a photoinduced current can be measured using a simple multimeter.[145] The calibrated photodiode was also used to measure the reflected light from the heterogenous solution and photoreactor.

## Applications of Formate

Formate is an anion of formic acid with the structure shown in Figure 8.

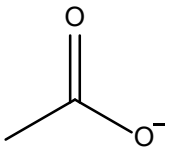

Figure 8. Structure of formate

Formate is one of the major products obtained from the reduction of $CO_2$.[146] One industrial application is the formate brine system (containing potassium, sodium, or cesium formate).[75,147] A formate brine system has been reportedly used in stabilization of xanthan gum, a polysaccharide used in drilling and completion fluids.[75] This is due to the ability of the formate brine system to stabilize biopolymer viscosity at temperature up to 200 $^oC$.[75] Also, formate brine systems are less corrosive, biodegradable, and have high stability towards shales.[76,77] Another important use of formate is a feedstock for direct liquid fuel cells (DLFCs).[78,148] An example is the direct formate-peroxide fuel cell (DFPFC), which consists of an alkaline formate anode and an acid-peroxide cathode. The reaction at the cathode and anode of a DFPFC are given in Equations 1.24-1.26.[148]

At the anode, formate is oxidized to $CO_3^{2-}$ and $H_2O$.

$$HCOO^- + 3\ OH^- \rightleftharpoons CO_3^{2-} + 2\ H_2O + 2e^- \qquad E^o \text{ anode} = -1.05V \qquad (1.24)$$

At the cathode, $H_2O_2$ is reduced to $H_2O$.

$$H_2O_2 + 2\ H^+ + 2e^- \rightleftharpoons 2\ H_2O \qquad E^o \text{ cathode} = 1.78V \qquad (1.25)$$

The overall redox reaction in the DFPFC is:

$$HCOO^- + OH^- + H_2O_2 \rightleftharpoons CO_3^{2-} + 2\ H_2O \quad E^o \text{ overall} = 2.83V \qquad (1.26)$$

The DFPFC has a high-power density of 331 $mWcm^{-2}$ at 60 $^oC$.[78,148]

Also, formate has been applied in fast pyrolysis of lignin.[79] Lignin, a major biomass component is a valuable material for producing other chemicals such as alkylphenols and aromatics.[79] Thermal degradation of lignin is difficult due to its complicated structure.[80] During fast pyrolysis process of lignin, addition of formate results in deoxyhydrogenation of lignin, removing methoxy groups from lignin and increasing contents of alkylphenols and aromatics.[79] Another key application of formate is biofuel synthesis.[149] This occurs in anaerobic systems where $CO_2$ is converted to formate by formate dehydrogenase, and subsequently to methane as a biofuel through a multistep pathway called methanogenesis.[149]

## Research Goals

The goal of this research is to develop a simple system for the photoreduction of carbon dioxide and to quantify the formate produced by ion chromatography (IC). This study examined use of metal phthalocyanines (copper, nickel, zinc and indium) as catalysts adsorbed to anatase $TiO_2$. Conditions such as pH and luminous intensity were varied to determine the effect on the amount of formate generated. A simple photodiode and integrating sphere absorbance measurements were used to determine the quantum yield.

# CHAPTER 2

## EXPERIMENTAL

### Materials and Equipment

The crystalline titanium dioxide (anatase) was purchased from Spectrum Chemical. Nickel phthalocyanine (purple) was purchased from Alfa Aesar, indium phthalocyanine (purple) from Sigma-Aldrich, zinc phthalocyanine (purple) and copper phthalocyanine (deep blue) were obtained from VWR Analytical. The oxidation state of In is 3+, while Zn, Ni, Cu have oxidation states of 2+. Sulfuric acid (98%) was purchased from Acros Organics. Carbon dioxide was obtained from Airgas with a purity of 99.7%.

### Photoreduction Experiment

The photoreduction experiment uses a paste formed by mixing 4.0-5.0 mg of metal phthalocyanine sensitizer and 0.5 g titanium dioxide using 2-3 drops of chloroform. The supported photocatalyst was transferred into a reactor using 50.0 mL of an aqueous 1.0 mM sulfuric acid solution and saturated by bubbling pure carbon dioxide into the solution for 30 min. The reactor was sealed with a stopper and placed about 50 cm from a simple 150 W incandescent light source. A water filter was used to absorb heat. Photoreduction was carried out while stirring magnetically. The irradiated solution, 10.0 mL, was centrifuged to remove titanium dioxide and metal phthalocyanine. A 20.0 μL sample was analyzed by ion chromatography every 24 h for 96 h. Peak area was used to quantify formate in ppm. Each experimental trial was repeated at least three times using fresh $TiO_2$ and sensitizer. The amount of formate in ppm was averaged and reported with standard deviations. Figure 9 below shows the experimental set-up.

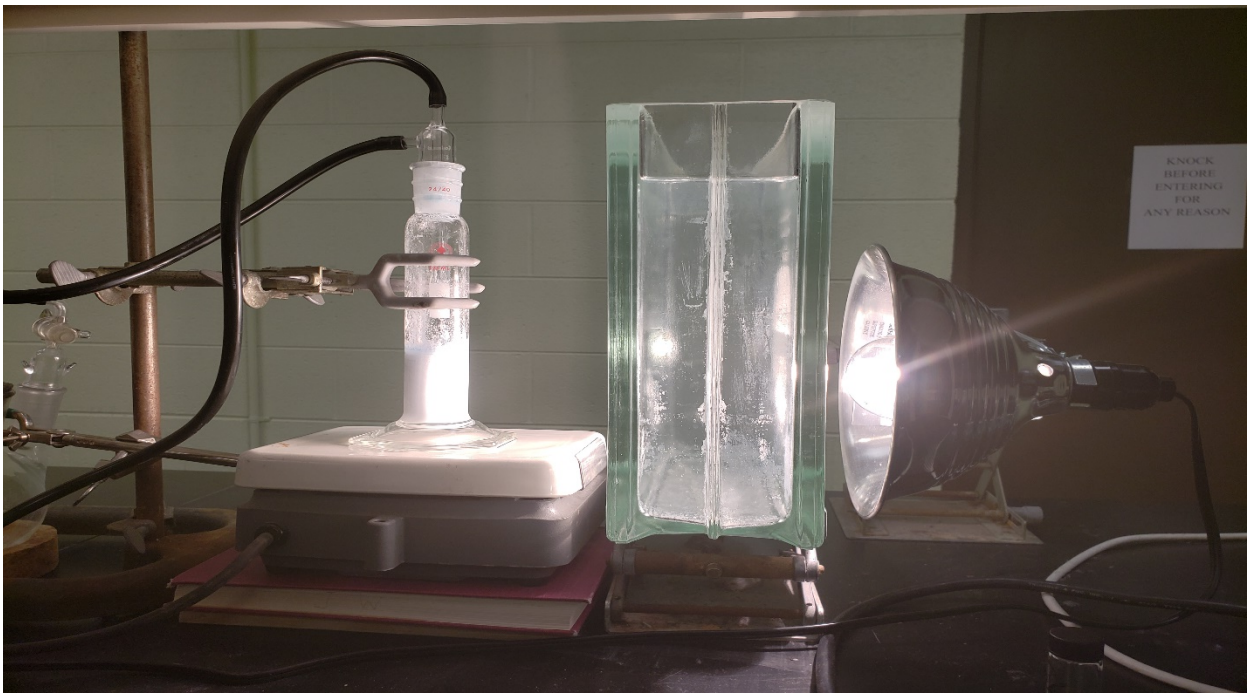


Figure 9. Photoreduction experimental setup (Photographed by Ovuokenye Omadoko)

## Preparation of Blank

The first blank was $TiO_2$, the sensitizer and 1.0 mM $H_2SO_4$ saturated with $CO_2$. A second blank was prepared using a mixture of 0.5 g $TiO_2$ and 50 mL of 1.0 mM sulfuric acid saturated with $CO_2$ but without sensitizer and illuminated. A third blank was prepared using a mixture of 4.0-5.0 mg metal phthalocyanine, 50 mL 1.0 mM $H_2SO_4$ saturated with $CO_2$ but without $TiO_2$ and illuminated. All blanks were stirred for 96 h.

## Calibration of Ion Chromatography

Formate analysis was determined by an ion chromatography. A 930 IC Flex System was obtained from Metrohm. Sodium carbonate, 3.6 mM, was used as the eluent with a flow rate of 0.7 mL/min and sulfuric acid 0.5 M (Acros Organics) as a regenerant. A 1,000 ppm formate stock solution was purchased from VWR Analytical.

The IC was calibrated using 50.0 ppm, 10.0 ppm, 5.00 ppm, and 1.00 ppm formate standards prepared in 1.0 mM sulfuric acid. Formate standards were injected using a 10.0 mL syringe to fill a 20 µL sample loop. The retention time for formate was found to be 4-5 min. Peak areas for the formate standards were used to generate a calibration curve. Figure 10 is a photo of the IC instrument.

Figure 10. Metrohm 930 IC instrument (Photographed by Ovuokenye Omadoko)

pH Measurement

To determine the change in hydrogen ion concentration of the acidic medium used over 96 h, pH measurements were performed using a Vernier pH probe calibrated with pH 4.0 and 7.0 buffer solutions. The pH measurements were performed before irradiation with light and at 24 h intervals during the photoreduction process.

Also, the effect of pH on reduction was explored. A solution of 1.0 M NaOH was used to adjust pH from 3.0 to 5.0 before combining with ZnPC, $TiO_2$ and saturated with $CO_2$ for 30 min. The mixture was illuminated using 150 W incandescent light source for 96 h. Formate yield was

quantified using IC at 24 h intervals. The procedure was repeated using pure water at a pH of 7.0 and 1.0 mM NaOH having a pH of 11.0.

## Light Intensity Variation

To determine the effect of light intensity on the yield of formate, mixtures of 0.5 g $TiO_2$, 5.0 mg ZnPC, and 50 mL 1.0 mM sulfuric acid was saturated $CO_2$ and illuminated with a 45 W, 150 W, 200 W incandescent light source for 24 h. All incandescent light sources had a color temperature of 2800 K. The temperature of 50 mL of water was measured using each light source. Due to warming of the solution and to determine if heat resulted in reduction of $CO_2$, the experiment was repeated at a constant temperature of 26.00±(0.01) °C using a temperature-controlled water bath without irradiation for 24 h.

## Visible Absorbance Studies

To determine the visible absorption spectrum of each MPC, 5.0 mg was stirred in 25 mL of toluene. A quartz cell of optical path length of 1 cm was filled with solution and absorbance measurement within the visible region was carried out using a SpectroVis Plus Spectrophotometer. Also, 0.5 g $TiO_2$ mixed with 10.0 mg InPC using 2 drops of chloroform was transferred into the reactor using 50 mL 1.0 mM $H_2SO_4$ and irradiated for 24 h. About 3 ml of solution was transferred into a test tube. Procedure was repeated using 0.5 g $TiO_2$ with 20 mg, 30 mg, 50 mg InPC respectively. 0.5 g $TiO_2$ in 50 mL of 1.0 mM $H_2SO_4$ was used as reference. All test tubes containing solution were sent to East Central University, Ada, Oklahoma for diffuse UV-Vis reflectance absorption measurements. This work was performed by Dr. Dwight Myers using a Perkin Elmer Lambda 35 UV-Vis Spectrophotometer using an integrated sphere.

## Quantum Yield Measurement

The quantum yield of formate involved determining the number of moles of formate generated and the number of absorbed photons. Incident photons from the 150 W incandescent light source was determined using a Hamamatsu S2387 33R Si photodiode with a surface area of 5.7 $mm^2$. Actinometry using a potassium iron oxalate solution was used to calibrate the photodiode as a visible polychromatic photon counter.[145] This method works by photons being absorbed resulting in oxidation of oxalate to $CO_2$ and reduction of $Fe^{3+}$ to $Fe^{2+}$. Iron 1,10-phenanthroline forms an orange complex with $Fe^{2+}$ and an absorbance measurement at 514 nm, volume of solution and time of radiation permit calculating photons emitted per second. A calibrated monochromator was used to isolate radiation at 514.0 ± 0.2 nm from the light source for which the quantum yield of the potassium iron oxalate solution is known to be 0.93. While this wavelength is not near the wavelength of maximum absorbance for phthalocyanines, approximately 680 nm, the sensitivity of the photodiode is 0.2 A/W and 0.5 A/W at 400 and 800 nm respectively. Assuming an ideal sensitivity of 0.5 A/W across the visible range, an area ratio of the sensitivity of the photodiode in this region can correct for the number photons measured by the photodiode. This area ratio is used to correct the constant for the photodiode in units of einsteins$\cdot A^{-1}\cdot s^{-1}$. Measuring the photodiode current can be used to determine the number of emitted photons. A 0.2 M potassium ferrioxalate solution was prepared by mixing 4.2 g KOH, 0.262 g $FeCl_3$ and 3.375 g oxalic acid ($H_2C_2O_4$) in the dark. Additional $H_2C_2O_4$ was added until a clear green solution of $K_3Fe(C_2O_4)_3$ was obtained. The green solution was diluted to 1.0 L with 5.16 g concentrated sulfuric acid and water. A buffer solution (pH = 5.0) was also prepared by mixing 24.8 g NaOH with 60.3 g glacial acetic acid and diluted to 1.0 L.

The potassium iron oxalate solution, 1.1 mL, was added to a beaker with 4.1 mL 0.1% 1,10-phenathroline solution, 0.61 mL buffer solution and diluted with 4.5 mL deionized water serving as

blank. The procedure was repeated illuminating approximately 3.5 mL of the $K_3Fe(C_2O_4)_3$ solution for 5 h with a calibrated monochromator set at 514 nm. Of the 3.5 mL, 1.2 mL was mixed with 4.1 mL 0.1% 1.10-phenathroline solution, 1.0 mL buffer solution and 4.1 mL deionized water. This solution results in the iron 1,10-phenanthroline complex which absorbs light at 514 nm. The absorbance of the blank and sample was measured at 514 nm, the wavelength of maximum absorbance for the iron phenanthroline complex. The difference in absorbance is used to calculate the number of emitted photons. The calibrated photodiode was used to measure the current generated when illuminated by the 150 W incandescent resulting in a current used for counting polychromatic photons.

The photodiode was also used to measure the reflected light from the heterogeneous solution and photoreactor. The current resulting from direct illumination of the photodiode and reflected were subtracted resulting in a current that was used to determine the number of true incident photons on the heterogeneous solution. The photodiode sensitivity increases nearly linearly from 0.2 A/W at 400 nm to 0.5 A/W at 800 nm. Assuming an ideal sensitivity of the photodiode (0.5 A/W) over this wavelength ranges, an area (A/W/nm) ratio was used to further correct the number of polychromatic photons.

Absorbance spectra using the integrated sphere technique were integrated to determine an area. The ratio of the difference in area of MPC/$TiO_2$ and $TiO_2$ only divided by MPC/$TiO_2$ multiplied by the number of true incident photons was used to determine the number of absorbed polychromatic photons. The quantum yield was calculated by taking two times the number of molecules of formate formed divided by the number of photons and multiplying by 100%.

# CHAPTER 3

# DATA AND RESULTS

## Calibration Curve Determination

Formate standards were analyzed using the IC instrument. Figure 11 shows the superimposed IC chromatograms obtained in which formate has a retention time of approximately 4-5 min and sulfate 16-20 min. The broad sulfate peak is most likely due to high concentration.

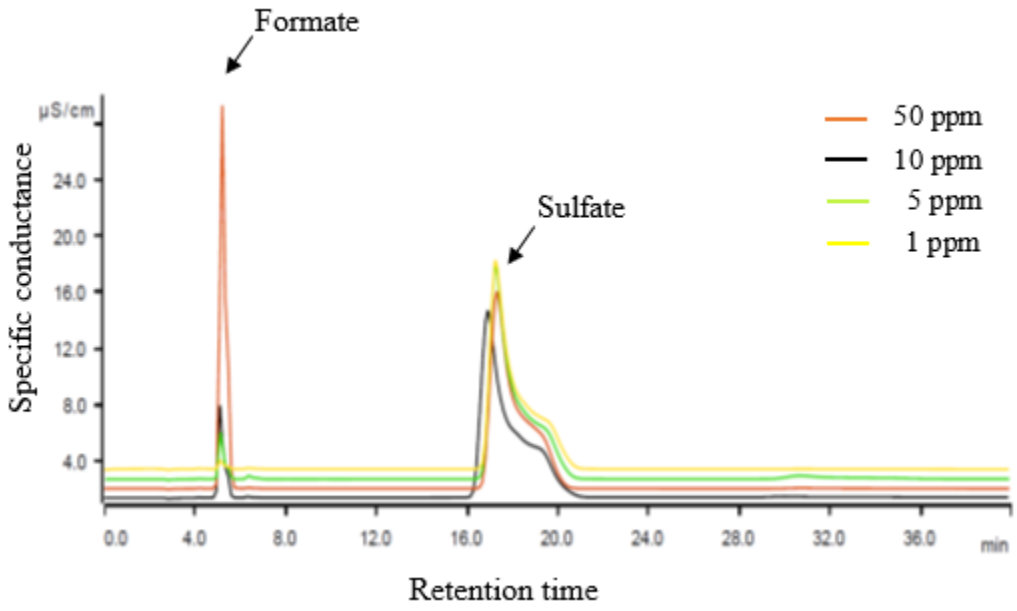


Figure 11. IC chromatograms of formate standard in 1.0 mM $H_2SO_4$

Table 1 lists the concentration of formate in 1.0 mM sulfuric acid and the peak areas obtained.

Table 1. Formate standard peak area

| Peak area (µS/cm*min) | Error (±µS/cm*min) | Concentration (ppm) |
|---|---|---|
| 8.242 | 0.015 | 50.0 |
| 1.916 | 0.004 | 10.0 |
| 0.893 | 0.009 | 5.0 |
| 0.168 | 0.016 | 1.0 |

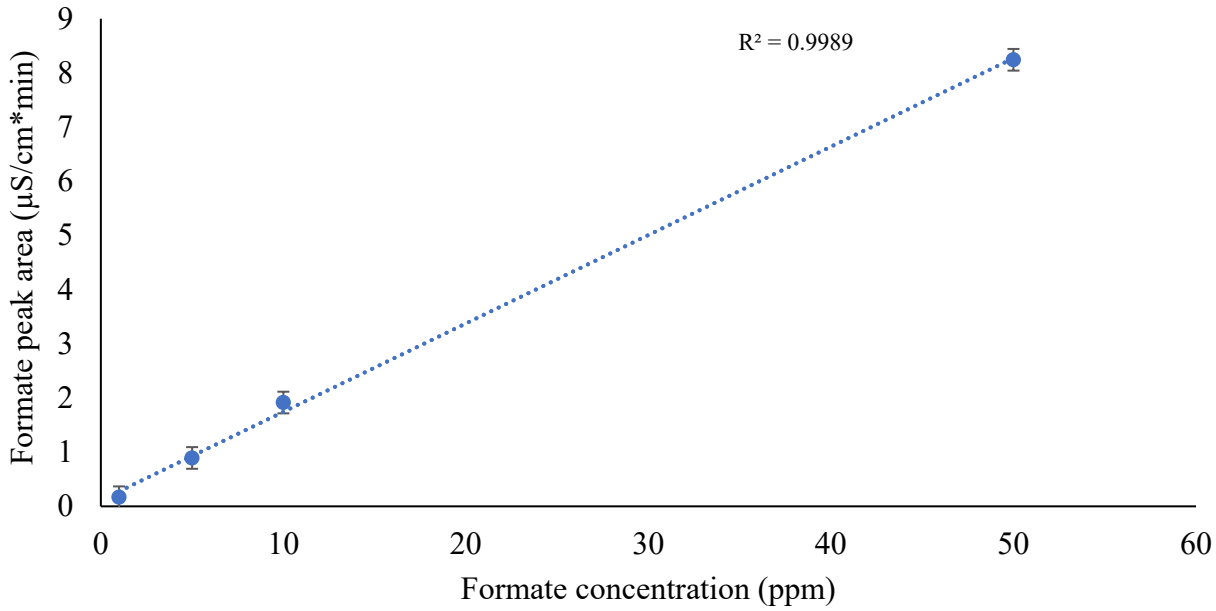


Figure 12. Calibration curve of IC using ppm formate standards in 1.0 mM $H_2SO_4$

A 1.00 ppm formate standard was measured four times to calculate the limit of detection and limit of quantitation. Three times the standard deviation and ten times the standard deviation of the peak area divided by the calibration slope resulted in a limit of detection of 0.289 ppm and limit of quantification of 0.964 ppm respectively.

## Blank Determination

Table 2 lists peak areas and concentration of formate obtained for the blank trials. All blank trials were analyzed after 96 h.

Table 2. The amount of formate determined in blank trials.

| Blank Trials | Peak area (μS/cm·min) | Concentration (ppm) |
|---|---|---|
| 1. ZnPC and $TiO_2$ in 1.0 mM $H_2SO_4$ saturated with $CO_2$, but no light irradiation. | ND | ND |
| 2. ZnPC in 1.0 mM $H_2SO_4$ saturated with $CO_2$ and light irradiation. | ND | ND |
| 3. $TiO_2$ in 1.0 mM $H_2SO_4$ saturated with $CO_2$ and light irradiation. | ND | ND |

ND - not detected.

## Effect of Sensitizer

Tables 3-6 show the effect of modifying $TiO_2$ with sensitizers CuPC, NiPC, ZnPC, and InPC on the amount of formate obtained. Table 6 shows that photoreduction of $CO_2$ to formate using InPC gave the highest amount of formate, 23.5 ppm. CuPC resulted in the lowest amount of formate after illumination for 96 h, 13.9 ppm.

Table 3. Amount of formate using CuPC/$TiO_2$.

| Irradiation time (h) | Peak area (μS/cm*min) | Concentration (ppm) | Trial |
|---|---|---|---|
| 96 | ND | ND | Dark |
| 0 | ND | ND | Light |
| 24 | 0.6(±0.1) | 3.6(±0.6) | Light |
| 48 | 1.2(±0.2) | 7.2(±1.2) | Light |
| 72 | 1.6(±0.4) | 9.6(±2.4) | Light |
| 96 | 2.3(±0.4) | 13.9(±2.4) | Light |

ND - not detected

Table 4. Amount of formate using NiPC/$TiO_2$.

| Irradiation time (h) | Peak area (μS/cm*min) | Concentration (ppm) | Trial |
|---|---|---|---|
| 96 | ND | ND | Dark |
| 0 | ND | ND | Light |
| 24 | 0.5(±0.2) | 3.0(±1.0) | Light |
| 48 | 1.5(±0.3) | 9.0(±1.8) | Light |
| 72 | 2.5(±0.3) | 15.0(±1.8) | Light |
| 96 | 3.2(±1.1) | 19.3(±6.6) | Light |

ND - not detected

Table 5. Amount of formate using ZnPC/$TiO_2$.

| Irradiation time (h) | Peak area (μS/cm*min) | Concentration (ppm) | Trial |
|---|---|---|---|
| 96 | ND | ND | Dark |
| 0 | ND | ND | Light |
| 24 | 1.1(±0.2) | 6.6(±1.2) | Light |
| 48 | 1.8(±0.5) | 11.0(±3.0) | Light |
| 72 | 2.8(±0.6) | 16.9(±3.5) | Light |
| 96 | 3.6(±0.3) | 21.7(±1.8) | Light |

ND - not detected

Table 6. Amount of formate using InPC/$TiO_2$.

| Irradiation time (h) | Peak area (μS/cm*min) | Concentration (ppm) | Trial |
|---|---|---|---|
| 96 | ND | ND | Dark |
| 0 | ND | ND | Light |
| 24 | 1.2(±0.2) | 7.2(±1.2) | Light |
| 48 | 2.2(±0.1) | 13.3(±0.6) | Light |
| 72 | 3.1(±0.8) | 18.7(±4.8) | Light |
| 96 | 3.9(±0.4) | 23.5(±2.4) | Light |

ND - not detected

Figure 13 shows variation of amount of formate produced at various time intervals using different MPC's.

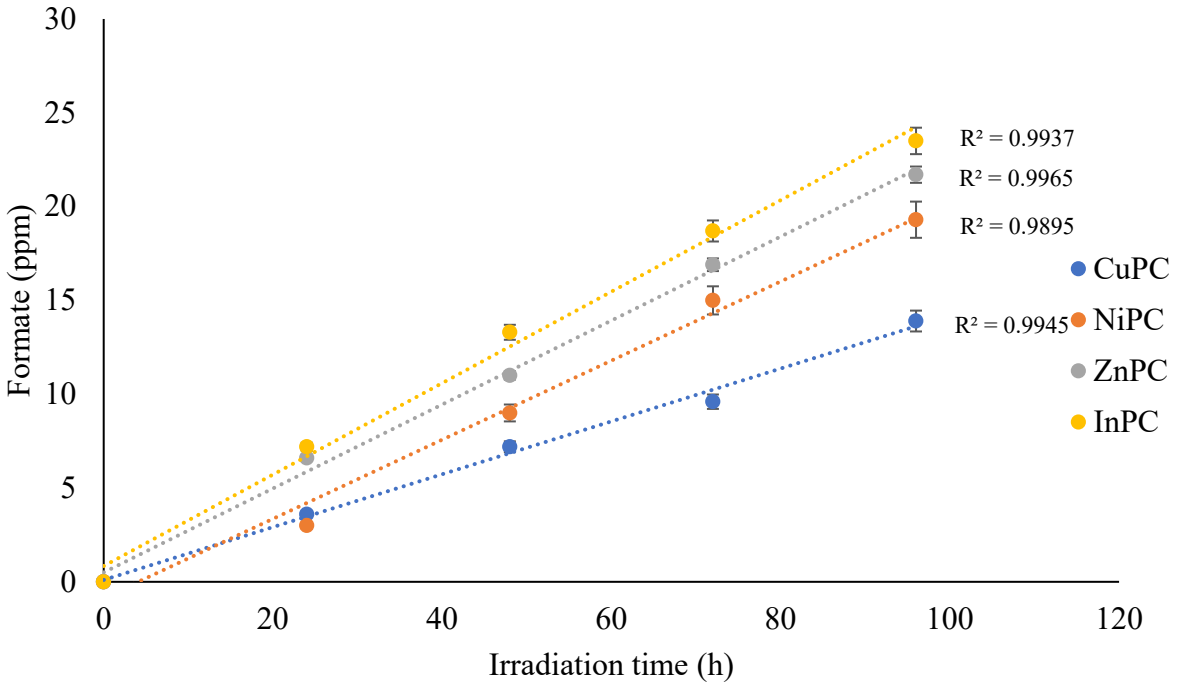


Figure 13. Graph of formate concentration vs irradiation time using different metal phthalocyanines

Table 7 and Figure 14 show the effect of modified $TiO_2$-InPC on the amount of formate obtained at pH 3.0 over 24 h.

Table 7**.** Effect of amount of sensitizer on formate production over 24 h at pH 3.0

| InPC (mg) | Formate Concentration (ppm) |
|---|---|
| 5.0 | 7.2(±1.5) |
| 10.0 | 3.6(±0.2) |
| 20.0 | 2.4(±0.4) |
| 50.0 | 1.8(±0.1) |

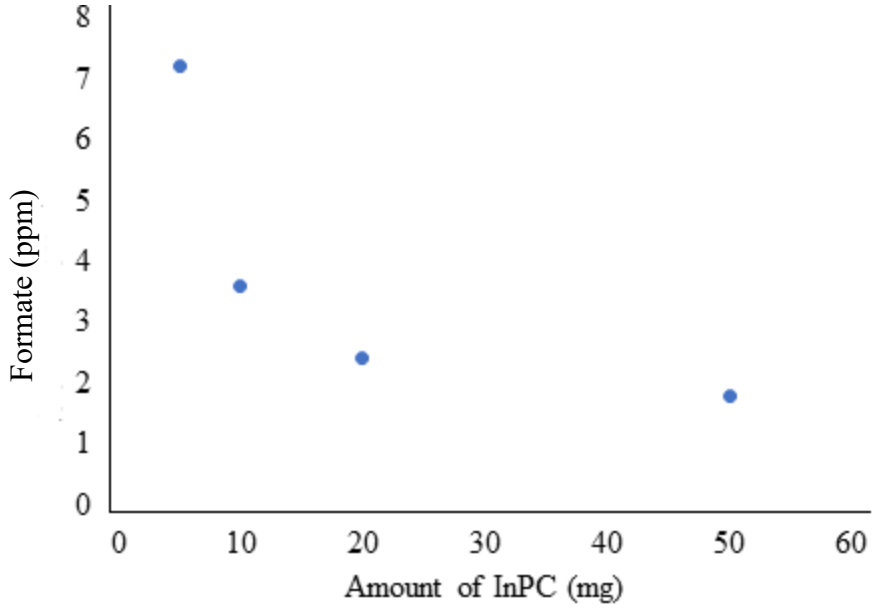


Figure 14. Amount of InPC (mg) vs formate concentration (ppm) over 24 h at pH 3.0

Amounts of InPC less than 5.0 mg will be used to determine the ratio of InPC and $TiO_2$ that results in a maximum amount of formate.

## Effect of Light Intensity

Table 8 shows the amount of formate obtained in photoereduction of $CO_2$ in 50 mL of 1.0 mM sulfuric acid with $TiO_2$ and ZnPC using 45, 150 and 200 W sources for 24 h as well as temperature.

Table 8. Amount of formate produce as a function of light intensity using ZnPC/$TiO_2$ over 24 h

| Source wattage (W) | Light intensity (lumens) | Formate Concentration (ppm) | Temperature (°C) |
|---|---|---|---|
| 45 | 350 | 0.3(±0.1) | 20.7 |
| 150 | 2740 | 6.6(±1.6) | 24.5 |
| 200 | 3880 | 8.2(±0.3) | 26.0 |
| 0 | 0 | ND | 26.0 |

ND is not detected

The temperature of the solution in the photoreactor does increases with the source intensity due to absorptive heating in the system. A reduction experiment was carried out in the dark at 26.0 °C. However, formate was not detected indicating that reduction of $CO_2$ is due to a photochemical or photo-thermal process. Figure 15 shows that the plot of formate produced and intensity is linear mostly within error using the 45, 150 and 200 W incandescent sources. A linear result is expected using low intensity sources.[150]

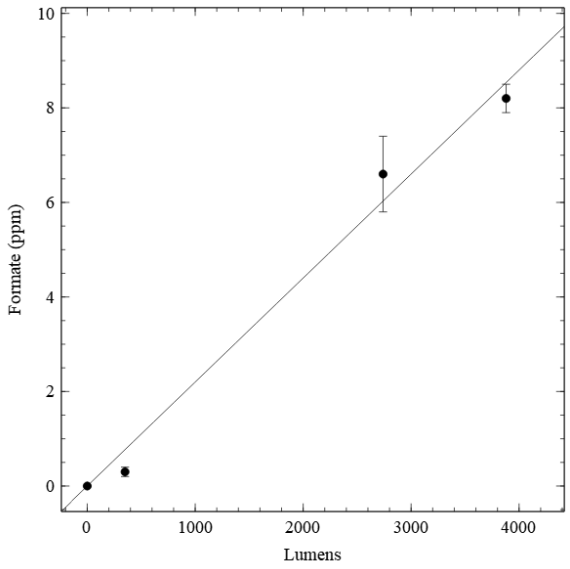


Figure 15. The amount of formate produced and luminous intensity over 24 h

Influence of pH on Photoreduction of Carbon Dioxide

The pH of the solution containing a mixture of saturated $CO_2$, $TiO_2$, ZnPC in 50 mL 1.0 mM sulfuric acid was measured before and after irradiation with a 150 W source. Table 9 and Figure 16 show the amount of formate produced under different pH conditions.

Table 9. Amount of formate produced using ZnPC at different pH.

| pH | Formate (ppm) 0 h | Formate (ppm) 24 h | Formate (ppm) 48 h | Formate (ppm) 72 h |
|---|---|---|---|---|
| 3.0 | ND | 6.6(±1.2) | 11.0(±3.0) | 16.9(±3.5) |
| 5.0 | ND | 1.3(±0.3) | 3.1(±0.9) | 5.8(±0.5) |
| 7.0 | ND | 1.2(±0.2) | 1.9(±1.1) | 3.8(±1.2) |
| 11.0 | ND | 1.6(±0.4) | 2.1(±0.7) | 4.8(±1.1) |

ND is not detected

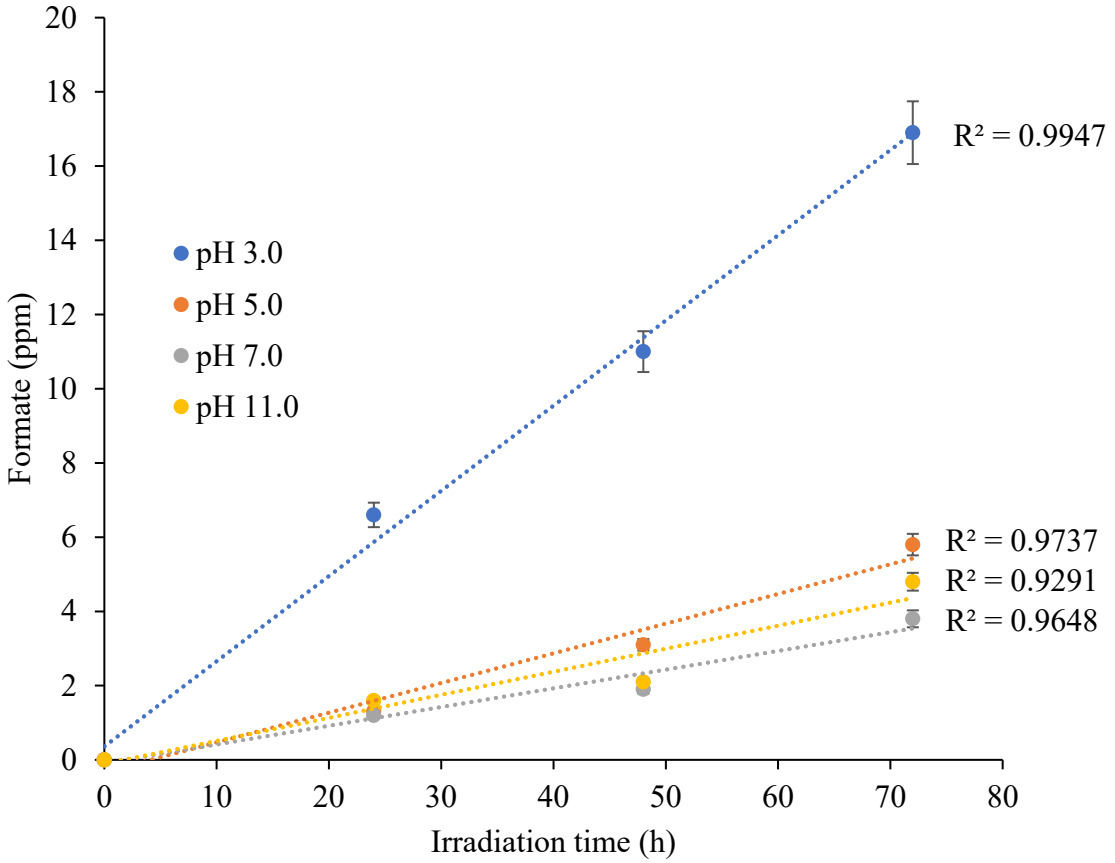


Figure 16. Graph of formate concentration vs irradiation time at different pH

## Visible Absorption Spectra of Metal Phthalocyanines

Figure 17 shows the visible absorption spectra of approximately 5 mg of CuPC, NiPC, ZnPC and InPC in 25 mL of toluene. All phthalocyanines measured show a Q and B band. In this work, only

the visible range of incident radiation is utilized. All MPC's have a maximum wavelength of absorption at approximate 680 nm.

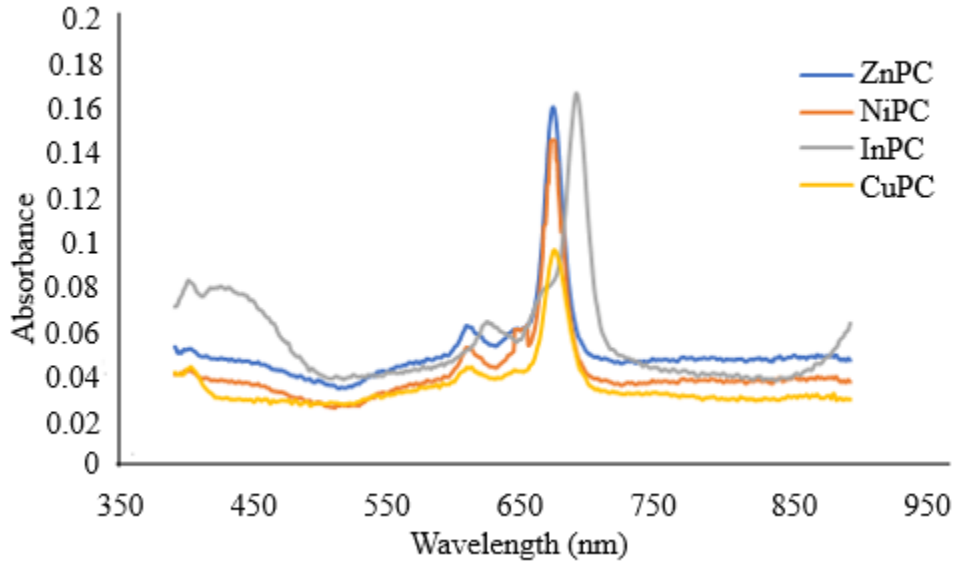


Figure 17. Visible absorption spectra of various MPCs

Visible Absorption Spectrum of Iron II Phenanthroline

Figure 18 shows the visible absorption spectrum of the green potassium iron (III) oxalate solution, and the iron (II) 1,10-phenanthroline complex formed on complexing free $Fe^{2+}(aq)$ ion with 1,10-phenanthroline solution. The wavelength of maximum absorption of potassium iron (III) oxalate in solution was found to be approximately 410 nm. The wavelength of maximum absorption of iron (II) 1,10-phenanthroline in solution is approximately 514 nm.

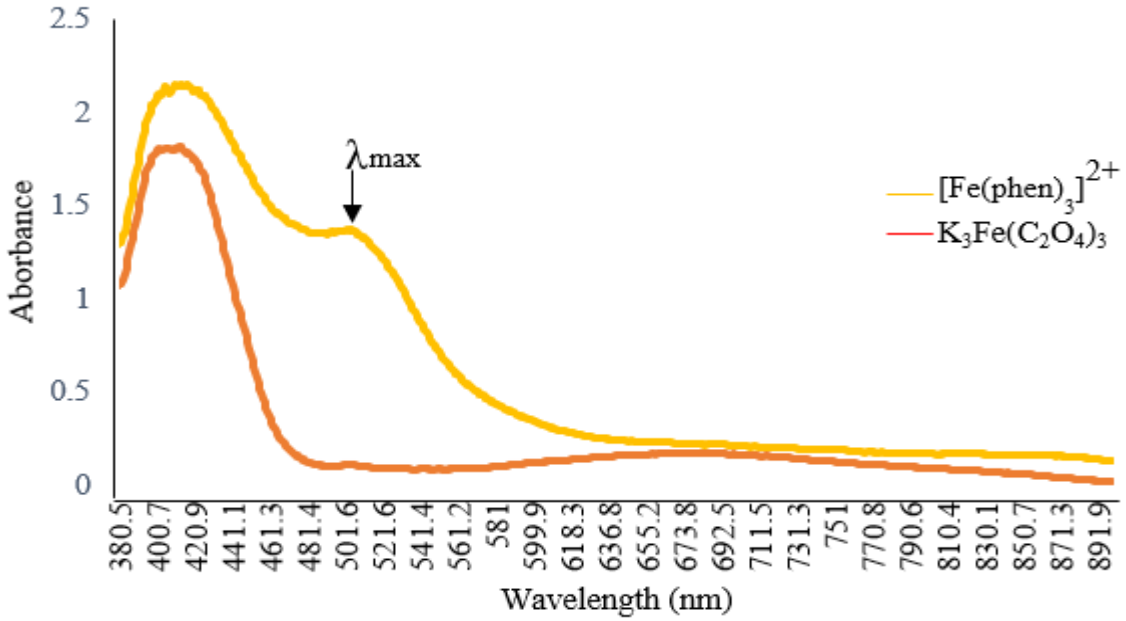


Figure 18. Visible absorption spectrum of potassium iron (III) oxalate and iron (II) 1,10-phenanthroline

Figure 19 shows the absorption spectra of various ratio of $TiO_2$/InPC loading using an integrated sphere.

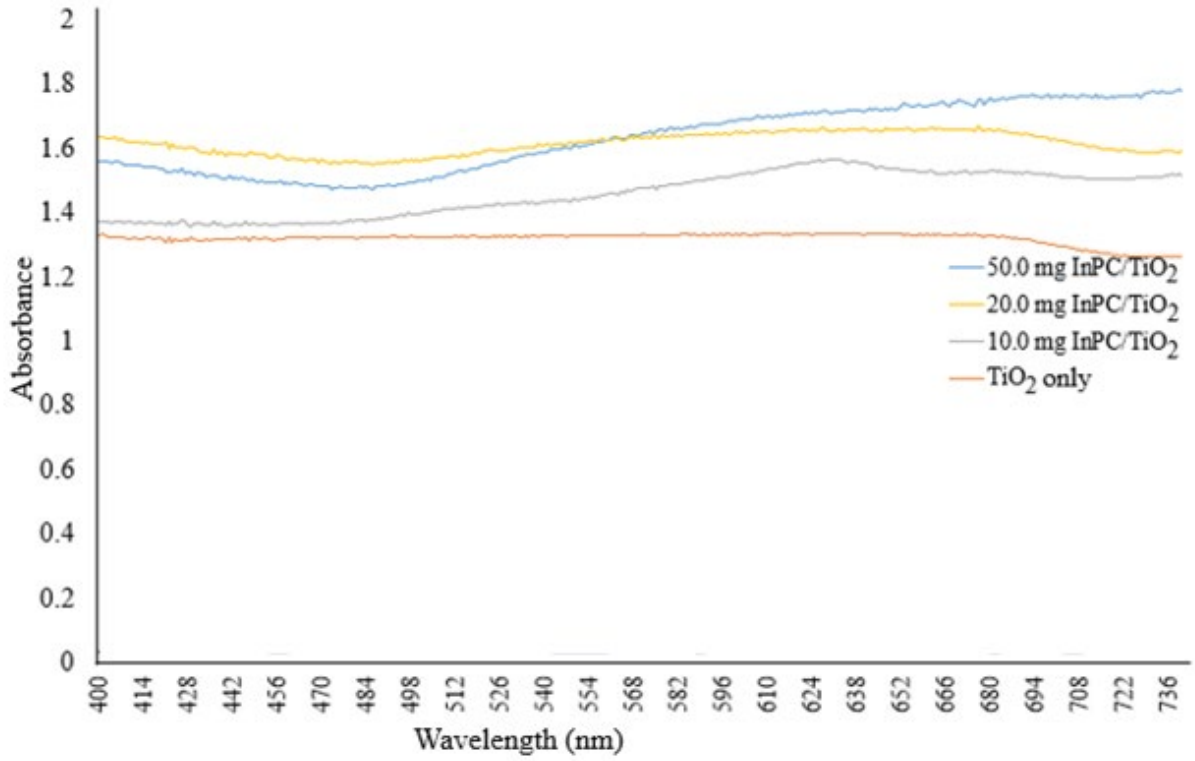


Figure 19. Absorption spectra of various ratios of $TiO_2$/InPC loading using an integrated sphere

The absorption area obtained using 0.5 g $TiO_2$/10 mg InPC and 0.5 g $TiO_2$ only in Figure 18 was integrated using logger pro 3.10.1 software within 350 nm–750 nm visible range.

Stoichiometric Yield Based on the Amount of Carbon Dioxide

Henry's law was used to determine a stoichiometric yield for formate based the amount of $CO_2$ in solution. Henry's law describes the relationship between partial pressure and aqueous concentration and is given in Equation 3.1.[23]

$$P_{CO_2} = k_H [CO_2]_{aq} \quad (3.1)$$

Where '$P_{CO_2}$' represents pressure of atmospheric $CO_2$ in atm, and '$k_H$' is Henry's constant for $CO_2$ in atm/M at room temperature (29 atm/M).[23] At 1.00 atm the concentration of aqueous $CO_2$ can be

calculated from Equation 3.0 and is 0.034 M. Equation 1.13 provides the stoichiometric ratio of $CO_2$ and formate allowing determination of the theoretical yield of formate provided in equation (3.2).

$$\left(\frac{0.034 \text{ mol } CO_2}{\text{L}}\right)\left(\frac{1 \text{ mol HCOOH}}{1 \text{ mol } CO_2}\right)\left(\frac{45.00 \text{ g}}{1 \text{ mol HCOOH}}\right)\left(\frac{1{,}000 \text{ mg}}{1 \text{ g}}\right) = 1{,}530 \text{ ppm formate} \qquad (3.2)$$

Using the experimental yield of formate after 96 h of illumination of the $TiO_2$/InPC system (23.5 ppm), and the theoretical yield of 1,530 ppm results in a stoichiometric yield of 1.54%.

## Quantum Yield

A Hamamatsu S2387 33R photodiode was calibrated using the potassium iron oxalate actinometry method using Equation 3.3.[145]

$$N_q = \frac{\Delta A \, V_1 \, V_3}{\Phi(\lambda) \, \varepsilon(514 \text{ nm}) \, V_2 \, l \, t} \qquad (3.3)$$

$N_q$ is moles of incident photons in einsteins per second. The quantity ΔA is the change in absorbance of the iron 1,10-phenanthroline complex before and after illumination. The term Φ(λ) is the quantum yield for reduction of $Fe^{3+}$ to $Fe^{2+}$ ion, which is 0.93 for a 0.2 M potassium iron oxalate solution using 514 nm radiation. The quantity $V_1$ is volume of $K_3Fe(C_2O_4)_3$ solution irradiated, $V_2$ is volume of solution analyzed after irradiation, $V_3$ is total volume of the solution after adding 0.1% 1,10-phenanthroline buffer solution and water, Ɛ (514 nm) is the molar absorption coefficient of the iron 1,10-phenanthroline complex (11,100 $L \cdot mol^{-1} \cdot cm^{-1}$), $l$ is optical pathlength and t is irradiation time in seconds.

Table 10. Absorbance values for three trials calibration the photodiode.

| Trial | Before Illumination Absorbance | After Illumination Absorbance |
|---|---|---|
| 1 | 0.103 | 0.169 |
| 2 | 0.103 | 0.186 |
| 3 | 0.103 | 0.181 |

For trial 1 using Equation 3.3, the number of moles of photons per second absorbed is given in Equation 3.4

$$\frac{(0.066)(3.5\ \text{mL} \times 10^{-3})(10.4\ mL)}{(0.93)(11{,}100\ Lmol^{-1}cm^{-1})(1.2\ \text{mL})(1\ cm)(18{,}000\ s)} = 1.1 \times 10^{-11}\ \text{einsteins}/s \quad (3.4)$$

The number of einsteins/s, the photodiode current measured (1.8 μA), given area of the photodiode (5.7 $mm^2$) and incident area of heterogeneous solution (3,500 $mm^2$) enabled determination of a constant such that current and number of incident polychromatic photons are proportional. Additionally, the change in intensity of the source as a function of wavelength and sensitivity of the photodiode means that the number of einsteins/s needs to be corrected. The photodiode increases in sensitivity linearly from 0.2 A/W at 400 nm to 0.5 A/W at 800 nm as given in the data sheet for the photodiode. Assuming an ideal sensitivity of 0.5 A/W across the visible range, an area ratio (0.7) of the sensitivity of the photodiode from approximately 400 to 800 nm corrects the current from the photodiode for counting polychromatic photons. These two ratios and the photodiode current were used to calculate the photodiode constant, $S_{\lambda,A}$, in einsteins/(A·s) given in Equation 3.5.

$$S_{\lambda,A} = \frac{(1.1 \times 10^{-11}\frac{\text{einsteins}}{\text{s}})(3{,}500\ \text{mm}^2)(0.7)}{(1.8\times10^{-6}\text{A})(5.7\ \text{mm}^2)} = 2.6 \times 10^{-3}\ \text{einsteins/(A·s)} \quad (3.5)$$

As such, the three trials calibrating the photodiode resulted in an average value of

$3.2 \pm 0.4 \times 10^{-3}$ einsteins/(A·s). The calibrated photodiode was illuminated directly by the 150 W incandescent source and the direct current (183 μA) was measured using a multimeter. The photodiode was also used to measure the reflected light from the heterogeneous solution and photoreactor (165 μA). However, the number of photons from the source varies with wavelength introducing error in the current measurement.[151] This error for the light source was determined by taking 18.27 lumens/Watt and dividing by 680 lumens/Watt, which is 100% luminous efficiency at

556 nm. The wavelength of 556 nm is the peak response of the human eye to visible light.[150] When this ratio is multiplied by the 150 W source 4.03 J/s is obtained. Assuming a near linear response of photons and wavelength from 400 to 740 nm, this corresponds to 1.2±0.4 x $10^{19}$ photons/s. The relative error on the number of photons is 33%. This relative error was applied to the current output of the photodiode and propagated to find the number of einsteins of photons absorbed. This calculation is shown in Equation 3.6.

$$(3.2 \pm 0.4 \times 10^{-3} \frac{einsteins}{A.S})(0.18 \pm 0.06 \times 10^{-4} A)(86{,}400\ s) = 5.0 \pm 1.8\ \times 10^{-3} einsteins \quad (3.6)$$

Integrated absorbance area from visible integrated sphere measurements of the MPC/$TiO_2$ solutions were used to determine the number of true incident photons absorbed. The areas for 0.5 g $TiO_2$ in 50 mL of 1.0 mM $H_2SO_4$ only and with 10, 20 and 50 mg of InPC were 811.27, 957.19, 984.68, and 1,086.85 respectively. To account for absorption of photons due to the added InPC only, the absorbance area of $TiO_2$ only was subtracted from the area with InPC and divided by the area of $TiO_2$ and InPC. Using 0.5 g $TiO_2$ and 10 mg InPC, the number of absorbed photons is given in Equation 3.7

$$(5.0 \pm 1.8\ \times 10^{-3} einsteins)(\frac{145.92}{957.19}) = \ 7.6 \pm 2.7\ \times 10^{-4} einsteins \quad (3.7)$$

From Table 7, the amount of formate obtained using 0.5 g $TiO_2$ with 5 mg of InPC and irradiation in 50 mL solution was determined to be 3.6(±0.2) ppm. The corresponding number of moles is given in Equation 3.8

$$\frac{(7.2 \pm 1.2\ mg)(1\ g)(1\ mol)(0.05\ L)}{(1\ L)(1000\ mg)(45\ g)} = \ 8.0 \pm 1.3 \times 10^{-6}\ mol\ formate \quad (3.8)$$

Considering that one einstein is a mole of photons, the quantum yield for formate obtained within 24 h of irradiation can be calculated as shown in Equation 3.9

$$\Phi_{\text{formate}} = \frac{2(8.0 \pm 1.3 \times 10^{-6} mol)}{(7.6 \pm 2.7\ x\ 10^{-4}\ einsteins)} \text{ x } 100\% \ = 2.1 \pm 0.8\% \quad (3.9)$$

The quantum yield of formate for using 0.5 g $TiO_2$ and 5 mg InPC was found to be 1.9 ± 0.7%, 1.8 ± 0.7% and 1.7 ± 0.6% after 48, 72 and 96 h of irradiation respectively. The results indicate that quantum yield is identical within error from 24 to 96 h of illumination.

# CHAPTER 4

# DISCUSSION AND CONCLUSIONS

From Figure 11, formate has a retention time between 4-5 min. Sulfate is also present due to sulfuric acid which has a retention time of 16-20 min. Table 1 shows that an increase in concentration of formate will lead to a corresponding increase in peak area of formate.

The calibration curve in Figure 12 was obtained by plotting peak area against concentration of formate and fit through the origin. The calibration was linear with an $R^2$ of 0.9989 given in Equation 4.1

$$A = 0.166C \tag{4.1}$$

Where A is the peak area in $\mu Scm^{-1}min^{-1}$ and C is concentration in ppm. Equation 4.1 above was used to find the concentration of formate generated by photoreduction of $CO_2$.

## Photoreduction of Carbon Dioxide to Formate

From Table 2, photoreduction of $CO_2$ to formate does not seem to occur when $TiO_2$ is used alone as a blank without a metal phthalocyanine. Titanium dioxide as a photocatalyst does not absorb radiation within the visible region, therefore it requires a sensitizer to extends its light absorption to visible region.[11,60,79,81] The metal phthalocyanine alone also results in an undetectable amount of formate. No formate was obtained using a catalyst and photosensitizer, without irradiation for 96 h. Tables 3-6 also show that the amount of formate generated in the dark is very low compared to the amount of formate when using visible radiation. The maximum amount of formate obtained after 96 h was 23.5 ppm formate using InPC. This result shows that light radiation is essential for reduction of $CO_2$ to formate in the photochemical process.

Although the presence of MPC catalyzes the photoreduction of $CO_2$ to formate, the $TiO_2$/MPC ratio is also key. According to Table 7 and Figure 14, higher amounts of InPC result in a decrease in the amount of formate. This could be due to a greater ratio of the amount of InPC to $TiO_2$ causing π stacking of InPC rings forming dimers which decreases absorbance and thus photochemical ability.[152]

## Effect of Luminous Intensity

From Table 8, after 24 h of irradiation, 0.3(±0.1) ppm formate was obtained using a 45 W light source. An increase in luminous intensity is consistent with an increase in the amount of formate produced. Also, no formate was obtained when the heterogenous solution was heated at 26 °C for 24 h without irradiation. This shows that the amount of heat absorbed by solution has no effect on photoreduction of $CO_2$ to formate. Reduction of CO2 to formate is clearly a photochemical or photo-thermal process.

## Effect of pH

The effect of pH of aqueous solution on the amount of formate produced was investigated using four different pH values (3, 5, 7, and 11). According to the results in Table 9 and Figure 15, there was no significant change in pH after illumination. This result obtained is probably due to a low amount of formate generated compared to theoretical yield of formate and resolution of the pH meter. As a result, photoreduction was carried out under acidic and basic conditions. The amount of formate decreases as pH approaches neutral conditions. A solution of pH 3.0 gave the highest yield of formate (16.6 ppm). Neutral pH resulted in the lowest amount of formate, (3.8 ppm). Photoreduction of $CO_2$ also occurs under alkaline conditions but the amount of formate is lower compared to acidic conditions. This result is consistent with literature.[133] This result may be

attributed to the difference in solubility and equilibrium of $CO_2$ in acidic, basic and neutral medium and desorption in acidic medium.[17,20]

## Use of Different MPC's

Figure 16 shows the visible absorption spectra of various MPCs used as photosensitizers. The Q-band absorption can be found within wavelengths of 650-750 nm in the visible region which is in accordance with literature.[105] The difference in absorbance of PCs is attributed the size of the metal center. A metal with a larger size will have weaker coordination to nitrogen in the phthalocyanine cause the difference between LUMO and HOMO to be smaller. This causes the wavelength of maximum absorbance to be longer.[108] This is observed in Figure 16. Figure 16 also shows that absorbance increases in the order of CuPC < NiPC < ZnPC < InPC. This is due to aggregation of MPC's.[152,153] Figure 13 reflects this trend in that the amount of formate generated is consistent with the order of increasing absorbance of the phthalocyanine. In other words, the amount of formate generated is greatest using InPC, followed by ZnPC, then NiPC while using CuPC resulted in the lowest amount of formate due to aggregation.

## Quantum Yield

The quantum yield was nearly 2.0%. Within error, quantum efficiency remains constant over time. The quantum yield is low but comparable to other systems.[140] Reasons for a low quantum yield include recombination of separated holes and electrons.[141] Photoreduction was done using a polychromatic incandescent light source while actinometry was used to calibrate a photodiode as a polychromatic photon counter. Direct illumination and reflected light by the heterogeneous solution and photoreactor was measured as a current using the photodiode. This introduces the largest uncertainty in the number of photons absorbed and available for photoreduction. Another source of

uncertainty is the area of solution receiving incident radiation as the photoreactor used has a curved surface.

## Rate of Reaction

Figure 13 shows plots of concentration and time exhibiting zero order kinetics for all phthalocyanines tested with $R^2$ values of 0.992 or higher. The rate of photoreduction of $CO_2$ to formate can be obtained from the slope of ppm vs. time for each metal phthalocyanine in Figure 13. The reaction rate constant is expressed as ppm formate (ppm) per second. Table 11 lists the reaction rates of photoreduction of $CO_2$ to formate using different metal phthalocyanine.

Table 11. Photochemical reduction reaction rates of $CO_2$ to formate using different metal phthalocyanines over 96 h.

| Metal phthalocyanine | Amount of formate (ppm) | Rate Constant (ppm/s) |
|---|---|---|
| CuPc | 13.9 ±2.4 | $4.0 \pm 0.7 \times 10^{-5}$ |
| NiPc | 19.3 ±6.6 | $5.6 \pm 1.9 \times 10^{-5}$ |
| ZnPc | 21.7 ±1.7 | $6.3 \pm 0.5 \times 10^{-5}$ |
| InPc | 23.5 ±2.9 | $6.8 \pm 0.8 \times 10^{-5}$ |

According to Table 11, photoreduction of $CO_2$ to formate using InPC and ZnPC, the photochemical reaction rate was statistically faster compared to use of NiPC and CuPC. The variation in the rate of formate produced using different sensitizers can be attributed to a different degree of aggregation in each phthalocyanine. InPC has the lowest degree of aggregation compared to other PC's used in this work. This results in a higher probability of $\pi$-$\pi^*$ transitions in InPC when illuminated with visible radiation.[98,105] The result is greater electron transfer to the conduction band of $TiO_2$ enhancing electron transfer reactions. This accounts for the greater amount of formate generated by InPC compared to NiPC, ZnPC and CuPC.

## Conclusions

Photoreduction of $CO_2$ to formate under acidic conditions using solid $TiO_2$ and MPC's is possible as quantified by ion chromatography. The amount of formate produced depends on wavelength, luminosity, metal sensitizer, pH, and time of radiation. The order of aggregation of sensitizers in solution used increases in the following manner: InPC > ZnPC > NiPC > CuPC. Aggregation of PCs limit the injection of electrons into the conduction band of the $TiO_2$ surface reducing electron transfer reactions.[105,153] Also, saturation of $CO_2$ in acidic medium gave higher yield when compared to basic or neutral conditions. Though photolysis of water produces protons required for the reduction process, more protons are present for photoreduction of $CO_2$ to formate under acidic conditions. The amount of formate increases over time with visible radiation. The quantum yield of photoreduction of $CO_2$ to formate was determined to be $2.1 \pm 0.8\%$ after 24 h and is a subject of ongoing research.

## Future Work

Photoreduction of $CO_2$ to formate should be extended to use of hydrophilic metal phthalocyanines such as tetrasulfophthaloycanines. Additionally, heteroleptic dimers may prove to be more active and selective toward photoreduction of $CO_2$. Amount of MPC/$TiO_2$ ratio required for maximum formate formation will also be investigated. Interestingly, use of UV-LED in combination with Visible LED sources in the Q and B bands of tetrasulfophthalocyanines are of interest for photoreduction experiments to improve quantum yield.

REFERENCES


(1) Roy, S. C.; Varghese, O. K.; Paulose, M.; Grimes, C. A. Toward Solar Fuels: Photocatalytic Conversion of Carbon Dioxide to Hydrocarbons. *ACS Nano* **2010**, *4* (3), 1259–1278.

(2) Biswas, P.; Wang, W.-N.; An, W.-J. The Energy-Environment Nexus: Aerosol Science and Technology Enabling Solutions. *Front. Environ. Sci. Eng. China* **2011**, *5* (3), 299.

(3) Lin, J.; Fridley, D.; Lu, H.; Price, L.; Zhou, N. Has Coal Use Peaked in China: Near-Term Trends in China's Coal Consumption. *Energy Policy* **2018**, *123*, 208–214.

(4) Suárez-Ruiz, I.; Crelling, J. C. *Applied Coal Petrology: The Role of Petrology in Coal Utilization*; Academic Press, 2008.

(5) Team, E. W. NOAA/ESRL Global Monitoring Division-The National Oceanic and Atmospheric Administration Annual Greenhouse Gas Index (AGGI). **2005**.

(6) He, J.-K. China's INDC and Non-Fossil Energy Development. *Adv. Clim. Chang. Res.* **2015**, *6* (3–4), 210–215.

(7) Psomopoulos, C. S.; Bourka, A.; Themelis, N. J. Waste-to-Energy: A Review of the Status and Benefits in USA. *Waste Manag.* **2009**, *29* (5), 1718–1724.

(8) Laing, D.; Bahl, C.; Bauer, T.; Lehmann, D.; Steinmann, W.-D. Thermal Energy Storage for Direct Steam Generation. *Sol. Energy* **2011**, *85* (4), 627–633.

(9) Olajire, A. A. $CO_2$ Capture and Separation Technologies for End-of-Pipe Applications–a Review. *Energy* **2010**, *35* (6), 2610–2628.

(10) Letcher, T. M. Why Do We Have Global Warming? In *Managing Global Warming*; Elsevier, 2019; pp 3–15.

(11) Quadrelli, E. A.; Centi, G.; Duplan, J.; Perathoner, S. Carbon Dioxide Recycling: Emerging Large-scale Technologies with Industrial Potential. *ChemSusChem* **2011**, *4* (9), 1194–1215.

(12) Aresta, M.; Dibenedetto, A. Utilisation of $CO_2$ as a Chemical Feedstock: Opportunities and Challenges. *Dalt. Trans.* **2007**, No. 28, 2975–2992.

(13) Min, X.; Kanan, M. W. Pd-Catalyzed Electrohydrogenation of Carbon Dioxide to Formate: High Mass Activity at Low Overpotential and Identification of the Deactivation Pathway. *J. Am. Chem. Soc.* **2015**, *137* (14), 4701–4708.

(14) Kopljar, D.; Inan, A.; Vindayer, P.; Wagner, N.; Klemm, E. Electrochemical Reduction of $CO_2$ to Formate at High Current Density Using Gas Diffusion Electrodes. *J. Appl. Electrochem.* **2014**, *44* (10), 1107–1116.

(15) Figueroa, J. D.; Fout, T.; Plasynski, S.; McIlvried, H.; Srivastava, R. D. Advances in $CO_2$ Capture Technology—the US Department of Energy's Carbon Sequestration Program. *Int. J. Greenh. gas Control* **2008**, *2* (1), 9–20.

(16) Chaffee, A. L.; Knowles, G. P.; Liang, Z.; Zhang, J.; Xiao, P.; Webley, P. A. $CO_2$ Capture by Adsorption: Materials and Process Development. *Int. J. Greenh. gas Control* **2007**, *1* (1), 11–18.

(17) Yu, C.-H.; Huang, C.-H.; Tan, C.-S. A Review of $CO_2$ Capture by Absorption and Adsorption. *Aerosol Air Qual. Res* **2012**, *12* (5), 745–769.

(18) Vega, F.; Cano, M.; Camino, S.; Navarrete, B.; Camino, J. A. Evaluation of the Absorption Performance of Amine-Based Solvents for $CO_2$ Capture Based on Partial Oxy-Combustion Approach. *Int. J. Greenh. Gas Control* **2018**, *73*, 95–103.

(19) Coenen, K.; Gallucci, F.; Hensen, E.; van Sint Annaland, M. Kinetic Model for Adsorption and Desorption of $H_2O$ and $CO_2$ on Hydrotalcite-Based Adsorbents. *Chem. Eng. J.* **2019**, *355*, 520–531.

(20) Ozdemir, E. Role of PH on $CO_2$ Sequestration in Coal Seams. *Fuel* **2016**, *172*, 130–138.

(21) Shokouhi, M.; Jalili, A. H.; Zoghi, A. T.; Ahari, J. S. Carbon Dioxide Solubility in Aqueous Sulfolane Solution. *J. Chem. Thermodyn.* **2019**, *132*, 62–72.

(22) Markham, A. E.; Kobe, K. A. The Solubility of Carbon Dioxide in Aqueous Solutions of Sulfuric and Perchloric Acids at 25. *J. Am. Chem. Soc.* **1941**, *63* (4), 1165–1166.

(23) Levy, J. B.; Hornack, F. M.; Levy, M. A. Simple Determination of Henry's Law Constant for Carbon Dioxide. *J. Chem. Educ.* **1987**, *64* (3), 260.

(24) Alvarez-Guerra, M.; Quintanilla, S.; Irabien, A. Conversion of Carbon Dioxide into Formate Using a Continuous Electrochemical Reduction Process in a Lead Cathode. *Chem. Eng. J.* **2012**, *207*, 278–284.

(25) Amatore, C.; Saveant, J. M. Mechanism and Kinetic Characteristics of the Electrochemical Reduction of Carbon Dioxide in Media of Low Proton Availability. *J. Am. Chem. Soc.* **1981**, *103* (17), 5021–5023.

(26) Inoue, T.; Fujishima, A.; Konishi, S.; Honda, K. Photoelectrocatalytic Reduction of Carbon Dioxide in Aqueous Suspensions of Semiconductor Powders. *Nature* **1979**, *277* (5698), 637.

(27) Dong, B.-X.; Wang, L.-Z.; Song, L.; Zhao, J.; Teng, Y.-L. Thermochemical Reduction of Carbon Dioxide with Alkali Metal Hydrides, Producing Methane and Hydrogen Fuels at Moderate Temperatures. *Energy & Fuels* **2016**, *30* (8), 6620–6625.

(28) Fujita, E.; Muckerman, J. T.; Himeda, Y. Interconversion of $CO_2$ and Formic Acid by Bio-Inspired Ir Complexes with Pendent Bases. *Biochim. Biophys. Acta (BBA)-Bioenergetics* **2013**, *1827* (8–9), 1031–1038.

(29) Alissandratos, A.; Kim, H.-K.; Easton, C. J. Formate Production through Carbon Dioxide Hydrogenation with Recombinant Whole Cell Biocatalysts. *Bioresour. Technol.* **2014**, *164*, 7–11.

(30) Kuwabata, S.; Tsuda, R.; Yoneyama, H. Electrochemical Conversion of Carbon Dioxide to Methanol with the Assistance of Formate Dehydrogenase and Methanol Dehydrogenase as Biocatalysts. *J. Am. Chem. Soc.* **1994**, *116* (12), 5437–5443.

(31) Laukel, M.; Chistoserdova, L.; Lidstrom, M. E.; Vorholt, J. A. The Tungsten-containing Formate Dehydrogenase from Methylobacterium Extorquens AM1: Purification and Properties. *Eur. J. Biochem.* **2003**, *270* (2), 325–333.

(32) Barin, R.; Biria, D.; Rashid-Nadimi, S.; Asadollahi, M. A. Enzymatic $CO_2$ Reduction to Formate by Formate Dehydrogenase from Candida Boidinii Coupling with Direct Electrochemical Regeneration of NADH. *J. $CO_2$ Util.* **2018**, *28*, 117–125.

(33) Kim, S.; Kim, M. K.; Lee, S. H.; Yoon, S.; Jung, K.-D. Conversion of $CO_2$ to Formate in an Electroenzymatic Cell Using Candida Boidinii Formate Dehydrogenase. *J. Mol. Catal. B Enzym.* **2014**, *102*, 9–15.

(34) Walcarius, A. Mesoporous Materials and Electrochemistry. *Chem. Soc. Rev.* **2013**, *42* (9), 4098–4140.

(35) Jitaru, M.; Lowy, D. A.; Toma, M.; Toma, B. C.; Oniciu, L. Electrochemical Reduction of

Carbon Dioxide on Flat Metallic Cathodes. *J. Appl. Electrochem.* **1997**, *27* (8), 875–889.

(36) Lv, W.; Zhang, R.; Gao, P.; Lei, L. Studies on the Faradaic Efficiency for Electrochemical Reduction of Carbon Dioxide to Formate on Tin Electrode. *J. Power Sources* **2014**, *253*, 276–281.

(37) Dutta, A.; Kuzume, A.; Rahaman, M.; Vesztergom, S.; Broekmann, P. Monitoring the Chemical State of Catalysts for $CO_2$ Electroreduction: An in Operando Study. *ACS Catal.* **2015**, *5* (12), 7498–7502.

(38) Liu, Y.; Chen, S.; Quan, X.; Yu, H. Efficient Electrochemical Reduction of Carbon Dioxide to Acetate on Nitrogen-Doped Nanodiamond. *J. Am. Chem. Soc.* **2015**, *137* (36), 11631–11636.

(39) Wu, J.; Risalvato, F. G.; Ke, F.-S.; Pellechia, P. J.; Zhou, X.-D. Electrochemical Reduction of Carbon Dioxide I. Effects of the Electrolyte on the Selectivity and Activity with Sn Electrode. *J. Electrochem. Soc.* **2012**, *159* (7), F353–F359.

(40) Singh, S. P.; Singh, P. Effect of Temperature and Light on the Growth of Algae Species: A Review. *Renew. Sustain. Energy Rev.* **2015**, *50*, 431–444.

(41) Šesták, Z. Blankenship, RE: Molecular Mechanisms of Photosynthesis. *Photosynthetica* **2002**, *40* (1), 12.

(42) Willows, R. D.; Li, Y.; Scheer, H.; Chen, M. Structure of Chlorophyll F. *Org. Lett.* **2013**, *15* (7), 1588–1590.

(43) Chen, M.; Blankenship, R. E. Expanding the Solar Spectrum Used by Photosynthesis. *Trends Plant Sci.* **2011**, *16* (8), 427–431.

(44) Chen, M. Chlorophyll Modifications and Their Spectral Extension in Oxygenic

Photosynthesis. *Annu. Rev. Biochem.* **2014**, *83*, 317–340.

(45) Gust, D.; Moore, T. A.; Moore, A. L. Solar Fuels via Artificial Photosynthesis. *Acc. Chem. Res.* **2009**, *42* (12), 1890–1898.

(46) Kodis, G.; Liddell, P. A.; De la Garza, L.; Clausen, P. C.; Lindsey, J. S.; Moore, A. L.; Moore, T. A.; Gust, D. Efficient Energy Transfer and Electron Transfer in an Artificial Photosynthetic Antenna− Reaction Center Complex. *J. Phys. Chem. A* **2002**, *106* (10), 2036–2048.

(47) Lu, H.; Yuan, W.; Zhou, J.; Chong, P. L.-G. Glucose Synthesis in a Protein-Based Artificial Photosynthesis System. *Appl. Biochem. Biotechnol.* **2015**, *177* (1), 105–117.

(48) Li, Y.; Scales, N.; Blankenship, R. E.; Willows, R. D.; Chen, M. Extinction Coefficient for Red-Shifted Chlorophylls: Chlorophyll d and Chlorophyll F. *Biochim. Biophys. Acta (BBA)-Bioenergetics* **2012**, *1817* (8), 1292–1298.

(49) Johnson, M. P. Correction: Photosynthesis. *Essays Biochem.* **2017**, *61* (4), 429.

(50) Silva, C. S.; Seider, W. D.; Lior, N. Exergy Efficiency of Plant Photosynthesis. *Chem. Eng. Sci.* **2015**, *130*, 151–171.

(51) El-Khouly, M. E.; El-Mohsnawy, E.; Fukuzumi, S. Solar Energy Conversion: From Natural to Artificial Photosynthesis. *J. Photochem. Photobiol. C Photochem. Rev.* **2017**, *31*, 36–83.

(52) Bishop, M. B.; Bishop, C. B. Photosynthesis and Carbon Dioxide Fixation. *J. Chem. Educ.* **1987**, *64* (4), 302.

(53) Muckerman, J.; Fujita, E. Artificial Photosynthesis. In *ACS Symposium Series*; American Chemical Society, 2009; Vol. 1025, pp 283–312.

(54) Bering, C. L. Energy Interconversions in Photosynthesis. *J. Chem. Educ.* **1985**, *62* (8), 659.

(55) Croft, H.; Chen, J. M.; Luo, X.; Bartlett, P.; Chen, B.; Staebler, R. M. Leaf Chlorophyll Content as a Proxy for Leaf Photosynthetic Capacity. *Glob. Chang. Biol.* **2017**, *23* (9), 3513–3524.

(56) Li, Y.; Cai, Z.-L.; Chen, M. Spectroscopic Properties of Chlorophyll F. *J. Phys. Chem. B* **2013**, *117* (38), 11309–11317.

(57) Chen, M.; Schliep, M.; Willows, R. D.; Cai, Z.-L.; Neilan, B. A.; Scheer, H. A Red-Shifted Chlorophyll. *Science (80-. ).* **2010**, *329* (5997), 1318–1319.

(58) Varghese, O. K.; Paulose, M.; LaTempa, T. J.; Grimes, C. A. High-Rate Solar Photocatalytic Conversion of $CO_2$ and Water Vapor to Hydrocarbon Fuels. *Nano Lett.* **2009**, *9* (2), 731–737.

(59) Shehzad, N.; Tahir, M.; Johari, K.; Murugesan, T.; Hussain, M. A Critical Review on $TiO_2$ Based Photocatalytic $CO_2$ Reduction System: Strategies to Improve Efficiency. *J. $CO_2$ Util.* **2018**, *26*, 98–122.

(60) Nozik, A. J. Photoelectrolysis of Water Using Semiconducting $TiO_2$ Crystals. *Nature* **1975**, *257* (5525), 383.

(61) Kumar, S. G.; Devi, L. G. Review on Modified $TiO_2$ Photocatalysis under UV/Visible Light: Selected Results and Related Mechanisms on Interfacial Charge Carrier Transfer Dynamics. *J. Phys. Chem. A* **2011**, *115* (46), 13211–13241.

(62) Zhang, H.; Banfield, J. F. Understanding Polymorphic Phase Transformation Behavior during Growth of Nanocrystalline Aggregates: Insights from TiO2. *J. Phys. Chem. B* **2000**, *104* (15), 3481–3487.

(63) Bourikas, K.; Kordulis, C.; Lycourghiotis, A. Titanium Dioxide (Anatase and Rutile): Surface Chemistry, Liquid–solid Interface Chemistry, and Scientific Synthesis of Supported Catalysts. *Chem. Rev.* **2014**, *114* (19), 9754–9823.

(64) Dambournet, D.; Belharouak, I.; Amine, K. Tailored Preparation Methods of $TiO_2$ Anatase, Rutile, Brookite: Mechanism of Formation and Electrochemical Properties. *Chem. Mater.* **2009**, *22* (3), 1173–1179.

(65) Davis, K. A. Titanium Dioxide. *J. Chem. Educ.* **1982**, *59* (2), 158.

(66) Hadjiivanov, K. I.; Klissurski, D. G. Surface Chemistry of Titania (Anatase) and Titania-Supported Catalysts. *Chem. Soc. Rev.* **1996**, *25* (1), 61–69.

(67) Yuenyongsuwan, J.; Nithiyakorn, N.; Sabkird, P.; Edgar, A. O.; Pongprayoon, T. Surfactant Effect on Phase-Controlled Synthesis and Photocatalyst Property of $TiO_2$ Nanoparticles. *Mater. Chem. Phys.* **2018**, *214*, 330–336.

(68) Rahimi, N.; Pax, R. A.; Gray, E. M. Review of Functional Titanium Oxides. I: $TiO_2$ and Its Modifications. *Prog. Solid State Chem.* **2016**, *44* (3), 86–105.

(69) Ola, O.; Maroto-Valer, M. M. Review of Material Design and Reactor Engineering on $TiO_2$ Photocatalysis for $CO_2$ Reduction. *J. Photochem. Photobiol. C Photochem. Rev.* **2015**, *24*, 16–42.

(70) Luttrell, T.; Halpegamage, S.; Tao, J.; Kramer, A.; Sutter, E.; Batzill, M. Why Is Anatase a Better Photocatalyst than Rutile?-Model Studies on Epitaxial $TiO_2$ Films. *Sci. Rep.* **2014**, *4*, 4043.

(71) Zhao, D.; Budhi, S.; Rodriguez, A.; Koodali, R. T. Rapid and Facile Synthesis of Ti-MCM-48

Mesoporous Material and the Photocatalytic Performance for Hydrogen Evolution. *Int. J. Hydrogen Energy* **2010**, *35* (11), 5276–5283.

(72) Carp, O.; Huisman, C. L.; Reller, A. Photoinduced Reactivity of Titanium Dioxide. *Prog. solid state Chem.* **2004**, *32* (1–2), 33–177.

(73) Thompson, R. *Industrial Inorganic Chemicals: Production and Uses*; Royal Society of Chemistry, 1995.

(74) Chambers, S. A.; Thevuthasan, S.; Farrow, R. F. C.; Marks, R. F.; Thiele, J. U.; Folks, L.; Samant, M. G.; Kellock, A. J.; Ruzycki, N.; Ederer, D. L. Epitaxial Growth and Properties of Ferromagnetic Co-Doped $TiO_2$ Anatase. *Appl. Phys. Lett.* **2001**, *79* (21), 3467–3469.

(75) Reinoso, D.; Martín-Alfonso, M. J.; Luckham, P. F.; Martínez-Boza, F. J. Rheological Characterisation of Xanthan Gum in Brine Solutions at High Temperature. *Carbohydr. Polym.* **2019**, *203*, 103–109.

(76) Downs, J. 'High Temperature Stabilization of Xanthan in Drilling Fluids by the Use of Formate Salts. *Phys. Chem. colloids interfaces oil Prod.* **1992**, *50*, 197–202.

(77) van Oort, E.; Hale, A. H.; Mody, F. K.; Roy, S. Critical Parameters in Modeling the Chemical Aspects of Borehole Stability in Shales and in Designing Improved Water-Based Shale Drilling Fluids. *SPE* **1994**, *28309*, 25–28.

(78) Li, Y. A Liquid-Electrolyte-Free Anion-Exchange Membrane Direct Formate-Peroxide Fuel Cell. *Int. J. Hydrogen Energy* **2016**, *41* (5), 3600–3604.

(79) Geng, J.; Wang, W.-L.; Yu, Y.-X.; Chang, J.-M.; Cai, L.; Shi, S. Q. Adding Nickel Formate in Alkali Lignin to Increase Contents of Alkylphenols and Aromatics during Fast Pyrolysis.

*Bioresour. Technol.* **2017**, *227*, 1–6.

(80) Zhang, M.; Resende, F. L. P.; Moutsoglou, A.; Raynie, D. E. Pyrolysis of Lignin Extracted from Prairie Cordgrass, Aspen, and Kraft Lignin by Py-GC/MS and TGA/FTIR. *J. Anal. Appl. Pyrolysis* **2012**, *98*, 65–71.

(81) Xue, L. M.; Zhang, F. H.; Fan, H. J.; Bai, X. F. Preparation of C Doped $TiO_2$ Photocatalysts and Their Photocatalytic Reduction of Carbon Dioxide. In *Advanced Materials Research*; Trans Tech Publ, 2011; Vol. 183, pp 1842–1846.

(82) Kim, J.; Choi, W.; Park, H. Effects of $TiO_2$ Surface Fluorination on Photocatalytic Degradation of Methylene Blue and Humic Acid. *Res. Chem. Intermed.* **2010**, *36* (2), 127–140.

(83) Asahi, R.; Morikawa, T.; Ohwaki, T.; Aoki, K.; Taga, Y. Visible-Light Photocatalysis in Nitrogen-Doped Titanium Oxides. *Science (80-. ).* **2001**, *293* (5528), 269–271.

(84) Ohno, T.; Akiyoshi, M.; Umebayashi, T.; Asai, K.; Mitsui, T.; Matsumura, M. Preparation of S-Doped $TiO_2$ Photocatalysts and Their Photocatalytic Activities under Visible Light. *Appl. Catal. A Gen.* **2004**, *265* (1), 115–121.

(85) Asahi, R.; Morikawa, T. Nitrogen Complex Species and Its Chemical Nature in $TiO_2$ for Visible-Light Sensitized Photocatalysis. *Chem. Phys.* **2007**, *339* (1–3), 57–63.

(86) Kumar, A.; Kumar, P.; Aathira, M. S.; Singh, D. P.; Behera, B.; Jain, S. L.; Stanbury, M.; Compain, J.-D.; Chardon-Noblat, S. A Bridged Ruthenium Dimer (Ru–Ru) for Photoreduction of $CO_2$ under Visible Light Irradiation. *J. Ind. Eng. Chem.* **2018**, *361*, 120–137.

(87) Krejčíková, S.; Matějová, L.; Kočí, K.; Obalová, L.; Matěj, Z.; Čapek, L.; Šolcová, O. Preparation and Characterization of Ag-Doped Crystalline Titania for Photocatalysis Applications. *Appl. Catal. B Environ.* **2012**, *111*, 119–125.

(88) Ni, M.; Leung, M. K. H.; Leung, D. Y. C.; Sumathy, K. A Review and Recent Developments in Photocatalytic Water-Splitting Using $TiO_2$ for Hydrogen Production. *Renew. Sustain. Energy Rev.* **2007**, *11* (3), 401–425.

(89) Kalyanasundaram, K.; Graetzel, M. Artificial Photosynthesis: Biomimetic Approaches to Solar Energy Conversion and Storage. *Curr. Opin. Biotechnol.* **2010**, *21* (3), 298–310.

(90) Cho, Y.; Choi, W.; Lee, C.-H.; Hyeon, T.; Lee, H.-I. Visible Light-Induced Degradation of Carbon Tetrachloride on Dye-Sensitized $TiO_2$. *Environ. Sci. Technol.* **2001**, *35* (5), 966–970.

(91) Mele, G.; Ciccarella, G.; Vasapollo, G.; García-López, E.; Palmisano, L.; Schiavello, M. Photocatalytic Degradation of 4-Nitrophenol in Aqueous Suspension by Using Polycrystalline $TiO_2$ Samples Impregnated with Cu (II)-Phthalocyanine. *Appl. Catal. B Environ.* **2002**, *38* (4), 309–319.

(92) Chen, X.; Mao, S. S. Titanium Dioxide Nanomaterials: Synthesis, Properties, Modifications, and Applications. *Chem. Rev.* **2007**, *107* (7), 2891–2959.

(93) Gupta, S. M.; Tripathi, M. A Review of $TiO_2$ Nanoparticles. *Chinese Sci. Bull.* **2011**, *56* (16), 1639.

(94) Dahlen, M. A. The Phthalocyanines a New Class of Synthetic Pigments and Dyes. *Ind. Eng. Chem.* **1939**, *31* (7), 839–847.

(95) Jeyalakshmi, V.; Mahalakshmy, R.; Krishnamurthy, K. R.; Viswanathan, B. Titania Based

Catalysts for Photoreduction of Carbon Dioxide: Role of Modifiers. **2012**.

(96) Słota, R.; Dyrda, G. UV Photostability of Metal Phthalocyanines in Organic Solvents. *Inorg. Chem.* **2003**, *42* (18), 5743–5750.

(97) Lomax, S. Q. Phthalocyanine and Quinacridone Pigments: Their History, Properties and Use. *Stud. Conserv.* **2005**, *50* (sup1), 19–29.

(98) Stuzhin, P. A.; Khelevina, O. G.; Berezin, B. D. In Phthalocyanines: Properties and Applications, Vol. 4, Leznoff CC and Lever ABP.(Eds.) VCH Publishers, Inc.: New York, 1996. *b) Stuzhin PA. J. Porphyrins Phthalocyanines* **1999**, *3*, 500–513.

(99) Aljuhani, A. A. Covalently Linked Dyads and Triads of Phthalocyanines and Porphyrins. University of East Anglia 2014.

(100) Hanack, M.; Heckmann, H.; Polley, R. 2. Phthalocyanines and Related Compounds. *Houben-Weyl, Methods Org. Chem. F Aromat. Heteroaromat. Large Rings* **1998**, 717–842.

(101) Thomas, A. L. *Phthalocyanine Research and Applications*; CRC Press, 1990.

(102) Robertson, J. M. 136. An X-Ray Study of the Structure of the Phthalocyanines. Part I. The Metal-Free, Nickel, Copper, and Platinum Compounds. *J. Chem. Soc.* **1935**, 615–621.

(103) Waring, D. R. Heterocyclic Dyes and Pigments. **1984**.

(104) Arslanoğlu, Y.; Sevim, A. M.; Hamuryudan, E.; Gül, A. Near-IR Absorbing Phthalocyanines. *Dye. Pigment.* **2006**, *68* (2–3), 129–132.

(105) Jia, N.; He, C.; Wang, S.; Song, W.; Chen, Z.; Zu, Y.; Gao, Y.; Dong, Y. Effect of Central Metals and Peripheral Substituents on the Third-Order Nonlinear Optical Properties of Tetra-Benzimidazole and Benzothiazole Substituted Phthalocyanines. *Opt. Mater. (Amst).* **2018**, *76*,

81–89.

(106) Tiwari, A.; Krishna, N. V.; Giribabu, L.; Pal, U. Hierarchical Porous $TiO_2$ Embedded Unsymmetrical Zinc–Phthalocyanine Sensitizer for Visible-Light-Induced Photocatalytic H2 Production. *J. Phys. Chem. C* **2017**, *122* (1), 495–502.

(107) Iagatti, A.; Doria, S.; Marcelli, A.; Angelini, N.; Notarantonio, S.; Paoletti, A. M.; Pennesi, G.; Rossi, G.; Zanotti, G.; Calogero, G. Photophysical Processes Occurring in a Zn-Phthalocyanine in Ethanol Solution and on $TiO_2$ Nanostructures. *J. Phys. Chem. C* **2015**, *119* (35), 20256–20264.

(108) Song, W.; He, C.; Dong, Y.; Zhang, W.; Gao, Y.; Wu, Y.; Chen, Z. The Effects of Central Metals on the Photophysical and Nonlinear Optical Properties of Reduced Graphene Oxide–metal (II) Phthalocyanine Hybrids. *Phys. Chem. Chem. Phys.* **2015**, *17* (11), 7149–7157.

(109) Skoog, D. A.; Leary, J. J. Principles of Instrumental Analysis Saunders. *New York* **1985**.

(110) Chen, J.; Gan, Q.; Li, S.; Gong, F.; Wang, Q.; Yang, Z.; Wang, S.; Xu, H.; Ma, J. S.; Yang, G. The Effects of Central Metals and Peripheral Substituents on the Photophysical Properties and Optical Limiting Performance of Phthalocyanines with Axial Chloride Ligand. *J. Photochem. Photobiol. A Chem.* **2009**, *207* (1), 58–65.

(111) Patel, D. G.; Feng, F.; Ohnishi, Y.; Abboud, K. A.; Hirata, S.; Schanze, K. S.; Reynolds, J. R. It Takes More than an Imine: The Role of the Central Atom on the Electron-Accepting Ability of Benzotriazole and Benzothiadiazole Oligomers. *J. Am. Chem. Soc.* **2012**, *134* (5), 2599–2612.

(112) Dent, C. E.; Linstead, R. P. 215. Phthalocyanines. Part IV. Copper Phthalocyanines. *J. Chem.*

*Soc.* **1934**, 1027–1031.

(113) Eberhardt, W.; Hanack, M. Synthesis of Hexadecaalkoxy-Substituted Nickel and Iron Phthalocyanines. *Synthesis (Stuttg).* **1997**, *1997* (01), 95–100.

(114) Yu, W.; Ye, M.; Zhu, J.; Wang, Y.; Liang, C.; Tang, J.; Tao, H.; Shen, Y. Zinc Phthalocyanine Encapsulated in Polymer Micelles as a Potent Photosensitizer for the Photodynamic Therapy of Osteosarcoma. *Nanomedicine Nanotechnology, Biol. Med.* **2018**, *14* (4), 1099–1110.

(115) Liu, W.; Jensen, T. J.; Fronczek, F. R.; Hammer, R. P.; Smith, K. M.; Vicente, M. G. H. Synthesis and Cellular Studies of Nonaggregated Water-Soluble Phthalocyanines. *J. Med. Chem.* **2005**, *48* (4), 1033–1041.

(116) Dhami, S.; Phillips, D. Comparison of the Photophysics of an Aggregating and Non-Aggregating Aluminium Phthalocyanine System Incorporated into Unilamellar Vesicles. *J. Photochem. Photobiol. A Chem.* **1996**, *100* (1–3), 77–84.

(117) Boyle, R. W.; van Lier, J. E. Synthesis of a Novel Water-Soluble Tetra [1-(O-Ethylphosphatobutyl)] Zinc Phthalocyanine. *Synthesis (Stuttg).* **1995**, *1995* (09), 1079–1080.

(118) Kasuga, K.; Hayashi, H.; Handa, M. Photoreduction of Methyl Viologen with a Water-Soluble Phthalocyaninatozinc (II) Complex in an Aqueous Solution. *Chem. Lett.* **1991**, *20* (11), 1877–1880.

(119) Li, X.; He, X.; Ng, A. C. H.; Wu, C.; Ng, D. K. P. Influence of Surfactants on the Aggregation Behavior of Water-Soluble Dendritic Phthalocyanines. *Macromolecules* **2000**, *33* (6), 2119–2123.

(120) Jeong, J.; Kumar, R. S.; Mergu, N.; Son, Y.-A. Photophysical, Electrochemical, Thermal and Aggregation Properties of New Metal Phthalocyanines. *J. Mol. Struct.* **2017**, *1147*, 469–479.

(121) Engelkamp, H.; Nolte, R. J. M. Molecular Materials Based on Crown Ether Functionalized Phthalocyanines. *J. Porphyr. Phthalocyanines* **2000**, *4* (05), 454–459.

(122) Ertem, B.; Yalazan, H.; Güngör, Ö.; Sarkı, G.; Durmuş, M.; Saka, E. T.; Kantekin, H. Synthesis, Structural Characterization, and Investigation on Photophysical and Photochemical Features of New Metallophthalocyanines. *J. Lumin.* **2018**, *204*, 464–471.

(123) Erdem, S. S.; Nesterova, I. V; Soper, S. A.; Hammer, R. P. Solid-Phase Synthesis of Asymmetrically Substituted "AB3-Type" Phthalocyanines. *J. Org. Chem.* **2008**, *73* (13), 5003–5007.

(124) BEKAROĞLU, Ö. History, Development, and a New Concept of Phthalocyanines in Turkey. *Turkish J. Chem.* **2014**, *38* (6), 903–922.

(125) Pandey, R. K.; Zheng, G. Porphyrins as Photosensitizers in Photodynamic Therapy. *Porphyr. Handb.* **2000**, *6*, 157–230.

(126) BEN-HUR, E.; CHAN, W.-S. Phthalocyanines in Photobiology and Their Medical Applications. In *The porphyrin handbook*; Elsevier, 2003; pp 1–35.

(127) Chaliha, S.; Bhattacharyya, K. G.; Paul, P. Catalytic Destruction of 4-chlorophenol in Water. *CLEAN–Soil, Air, Water* **2008**, *36* (5-6), 488–497.

(128) Pirbazari, A. E. Sensitization of Tio2 Nanoparticles With Cobalt Phthalocyanine: An Active Photocatalyst for Degradation of 4-Chlorophenol Under Visible Light. *Procedia Mater. Sci.* **2015**, *11*, 622–627.

(129) Yıldız, B.; Güzel, E.; Menges, N.; Şişman, İ.; Şener, M. K. Pyrazole-3-Carboxylic Acid as a New Anchoring Group for Phthalocyanine-Sensitized Solar Cells. *Sol. Energy* **2018**, *174*, 527–536.

(130) Ooyama, Y.; Harima, Y. Molecular Designs and Syntheses of Organic Dyes for Dye-sensitized Solar Cells. *European J. Org. Chem.* **2009**, *2009* (18), 2903–2934.

(131) He, H.; Gurung, A.; Si, L. 8-Hydroxylquinoline as a Strong Alternative Anchoring Group for Porphyrin-Sensitized Solar Cells. *Chem. Commun.* **2012**, *48* (47), 5910–5912.

(132) Linsebigler, A. L.; Lu, G.; Yates Jr, J. T. Photocatalysis on $TiO_2$ Surfaces: Principles, Mechanisms, and Selected Results. *Chem. Rev.* **1995**, *95* (3), 735–758.

(133) Mele, G.; Annese, C.; D'Accolti, L.; De Riccardis, A.; Fusco, C.; Palmisano, L.; Scarlino, A.; Vasapollo, G. Photoreduction of Carbon Dioxide to Formic Acid in Aqueous Suspension: A Comparison between Phthalocyanine/$TiO_2$ and Porphyrin/$TiO_2$ Catalysed Processes. *Molecules* **2015**, *20* (1), 396–415.

(134) Fukuzumi, S.; Lee, Y.-M.; Ahn, H. S.; Nam, W. Mechanisms of Catalytic Reduction of $CO_2$ with Heme and Nonheme Metal Complexes. *Chem. Sci.* **2018**, *9* (28), 6017–6034.

(135) Vasant Kumar, R.; Coto, M. Visible-Light-Active Photocatalysis: Nanostructured Catalyst Design, Mechanisms, and Applications. *Visible Light. Photocatal. Nanostructured Catal. Des. Mech. Appl.* **2018**, 499–526.

(136) Wang, W.-N.; Soulis, J.; Yang, Y. J.; Biswas, P. Comparison of $CO_2$ Photoreduction Systems: A Review. *Aerosol Air Qual. Res* **2014**, *14* (2), 533–549.

(137) Liu, S.; Zhao, Z.; Wang, Z. Photocatalytic Reduction of Carbon Dioxide Using Sol–gel

Derived Titania-Supported CoPc Catalysts. *Photochem. Photobiol. Sci.* **2007**, *6* (6), 695–700.

(138) Srinivas, B.; Shubhamangala, B.; Lalitha, K.; Anil Kumar Reddy, P.; Durga Kumari, V.; Subrahmanyam, M.; De, B. R. Photocatalytic Reduction of $CO_2$ over Cu-$TiO_2$/Molecular Sieve 5A Composite. *Photochem. Photobiol.* **2011**, *87* (5), 995–1001.

(139) Yotsuhashi, S.; Hashiba, H.; Deguchi, M.; Zenitani, Y.; Hinogami, R.; Yamada, Y.; Deura, M.; Ohkawa, K. Highly Efficient Photochemical HCOOH Production from $CO_2$ and Water Using an Inorganic System. *AIP Adv.* **2012**, *2* (4), 42160.

(140) Nakada, A.; Koike, K.; Nakashima, T.; Morimoto, T.; Ishitani, O. Photocatalytic $CO_2$ Reduction to Formic Acid Using a Ru (II)–Re (I) Supramolecular Complex in an Aqueous Solution. *Inorg. Chem.* **2015**, *54* (4), 1800–1807.

(141) Krýsa, J.; Baudys, M.; Mills, A. Quantum Yield Measurements for the Photocatalytic Oxidation of Acid Orange 7 (AO7) and Reduction of 2, 6-Dichlorindophenol (DCIP) on Transparent TiO2 Films of Various Thickness. *Catal. Today* **2015**, *240*, 132–137.

(142) Serpone, N. Relative Photonic Efficiencies and Quantum Yields in Heterogeneous Photocatalysis. *J. Photochem. Photobiol. A Chem.* **1997**, *104* (1–3), 1–12.

(143) Srinivasan, P. D.; Nitz, S. R.; Stephens, K. J.; Atchison, E.; Bravo-Suarez, J. J. Modified Harrick Reaction Cell for in Situ/Operando Fiber Optics Diffuse Reflectance UV–visible Spectroscopic Characterization of Catalysts. *Appl. Catal. A Gen.* **2018**, *561*, 7–18.

(144) Shelton, C. T. Integrating Sphere Functionality: The Scatter Transmission Measurement.

(145) Kuhn, H. J.; Braslavsky, S. E.; Schmidt, R. Chemical Actinometry (IUPAC Technical Report). *Pure Appl. Chem.* **2004**, *76* (12), 2105–2146.

(146) Amao, Y. Formate Dehydrogenase for $CO_2$ Utilization and Its Application. *J. $CO_2$ Util.* **2018**.

(147) Caenn, R.; Darley, H. C. H.; Gray, G. R. *Composition and Properties of Drilling and Completion Fluids*; Gulf professional publishing, 2011.

(148) Li, Y.; He, Y.; Yang, W. A High-Performance Direct Formate-Peroxide Fuel Cell with Palladium–gold Alloy Coated Foam Electrodes. *J. Power Sources* **2015**, *278*, 569–573.

(149) Kim, M.; Ahn, Y.-H.; Speece, R. E. Comparative Process Stability and Efficiency of Anaerobic Digestion; Mesophilic vs. Thermophilic. *Water Res.* **2002**, *36* (17), 4369–4385.

(150) Kočí, K.; Obalová, L.; Lacný, Z. Photocatalytic Reduction of $CO_2$ over $TiO_2$ Based Catalysts. *Chem. Pap.* **2008**, *62* (1), 1–9.

(151) https://web.archive.org/web/20120423123823/http://www.ccri.edu/physics/keefe/light.htm

(152) Sessler, J. L.; Jayawickramarajah, J.; Gouloumis, A.; Pantos, G. D.; Torres, T.; Guldi, D. M. Guanosine and Fullerene Derived De-Aggregation of a New Phthalocyanine-Linked Cytidine Derivative. *Tetrahedron* **2006**, *62* (9), 2123–2131.

(153) de Souza, T. F. M.; Antonio, F. C. T.; Zanotto, M.; Homem-de-Mello, P.; Ribeiro, A. O. Photophysical and Photochemical Properties and Aggregation Behavior of Phthalocyanine and Naphthalocyanine Derivatives. *J. Braz. Chem. Soc.* **2018**, *29* (6), 1199–1209.

# VITA

## OVUOKENYE OMADOKO

| | |
|---|---|
| Education | M.S. Chemistry, East Tennessee State University<br>Johnson City, TN, USA. (August 2019).<br>B.Sc. Industrial Chemistry, University of Benin,<br>Benin City, Edo, Nigeria. (December 2007). |
| Professional Experience | Graduate Teaching Assistant, East Tennessee State University,<br>Johnson City, TN, USA. January 2017 – December 2018.<br>Chemist, Nigerian Bottling Company PLC, Benin City, Nigeria.<br>May 2012- December 2016.<br>Chemistry Tutor, Assurance High School, Delta State, Nigeria,<br>January 2009-December 2011. |